EXOSPHERIC MODELS OF THE TOPSIDE IONOSPHERE

J. LEMAIRE and M. SCHERER

Belgian Institute for Space Aeronomy, B-1180, Brussels, Belgium

Abstract. The historical evolution of the study of escape of light gases from planetary atmospheres is delineated, and the application of kinetic theory to the ionsphere is discussed. Ionospheric plasma becomes collisionless above the ion-exobase which is located near 1000 km altitude in the trough and polar regions, and which coïncides with the plasmapause at lower latitudes. When the boundary conditions at conjugate points of a closed magnetic field line are different, interhemispheric particle fluxes exist from the high temperature point to the low temperature point, and from the point of larger concentrations to the point of smaller concentrations; therefore the charge separation electric field in the exosphere is no longer given by the Pannekoek-Rosseland field. For non-uniform number densities and temperatures at the exobase, the observed r^{-4} variation of the equatorial density distribution is recovered in the calculated density distributions. Taking account of plasmasheet particle precipitation does not change very much the electric field and ionospheric ion distributions, at least for reasonable densities and temperatures of the plasmasheet electrons and protons. For field aligned current densities along auroral field lines smaller than 10^{-5} Am^{-2}, the potential difference between the ion-exobase and plasmasheet is about -3V. In the case of open magnetic field lines the flow speed of hydrogen and helium ions in the exosphere becomes rapidly supersonic as a consequence of the upward directed charge separation electric field, whereas the oxygen ions have a negligible small bulk velocity. Adding a photoelectron efflux decreases the thermal electron escape but does not change significantly the number density distributions.

1. Introduction

The kinetic theory of planetary atmospheres is as old as the kinetic theory of gases itself. At the beginning only neutral planetary atmospheres were considered but later on the outermost regions of the ionosphere were also studied with the help of kinetic models. The purpose of this paper is to give a brief review of the applications of kinetic theory to the collision-free domains of the terrestrial atmosphere and more precisely to the ion-exosphere. The historical evolution of the basic ideas are given in Section 2. The ion-exobase location is discussed in Section 3. A comparison between the kinetic approach in the neutral and in the ion-exosphere, as well as between the kinetic theory and the CGL approximation is given in Section 4. Because of the existence of the magnetospheric tail a fundamental difference must be made between the low-latitude ionosphere and the polar ionosphere of the Earth. In the former case, which is discussed in Section 5, the electrons and ions move under the constraint of a dipole like magnetic field. In the polar regions however the magnetic field lines are open and hence the ionospheric particles, especially the protons, electrons and helium ions, can escape into the magnetotail. A kinetic description of this plasma flow, which is known as the polar wind will be discussed in Section 6. Finally the main results and conclusions are summarized in Section 7.

2. Historical Development

Although a comprehensive review of the escape of light gases from a planetary atmosphere is given by Chamberlain (1963), it will be good for the sake of completeness to

Space Science Reviews **15** (1974) 591–640.

recall the main steps in the evolution of neutral exosphere models, especially since most of the basic assumptions were resumed in the ion-exosphere models.

2.1. The neutral exosphere

In any planetary atmosphere collisions between the molecules and/or atoms become more and more infrequent with the radial distance as a consequence of the decrease of density with height. Hence there must exist a region where the mean free path becomes so large that collisions can be neglected. In this region the particles are describing 'free' paths of enormous dimensions. The existence of such a collision-free domain was first assumed by Stoney (1868) who also pointed out that due to the velocity dispersion of the molecules in the atmosphere, there always will be molecules with sufficiently large velocities to overcome the gravitational potential, even when the mean molecular velocity is smaller than the minimum speed of escape. Consequently such molecules will escape into the interplanetary space (Stoney, 1898). Nearly half a century before, the kinetic theory of escape was anticipated by Waterston (1846) who in his discussion 'On the Vertical Equilibrium of a Medium, Supposing it to Form the Atmosphere of a Planet' assumed that at a given height, all the molecular velocities are given by the root mean square velocity. It was only in 1892 that the full extend of Waterston's paper was published at the demand of Lord Rayleigh (Waterston, 1892).

Inspired by Stoney's papers and applying Maxwell's velocity distribution, Cook (1900) determined the relative number of molecules that will leave the atmosphere. Bryan (1900, 1901) modified the Maxwell-Boltzmann distribution in order to take account of axial rotation and he considered the problem of the stationary distribution of the molecules in the atmosphere of a rotating planet. In a series of subsequent papers, Stoney (1900a, b, c, 1904) impugned the method used by Cook and Bryan.

The rate of loss of planetary atmospheres was also studied by Jeans (1925) who assumed an isothermal atmosphere and a Maxwell-Boltzmann velocity distribution. In Jeans' formula of the escape flux, the radial distance of the spherical surface surrounding the planet outside which collisions are supposed to be infrequent, remains undetermined. Henceforward this spherical surface will be called the *exobase* or *baropause* and the height at which it is located is known as the *critical level*. The exosphere is the atmosphere above the critical level (Spitzer, 1949).

A first attempt to determine the exobase was made by Milne (1923) and Jones (1923), who based their calculations on a study of the collisional processes. They showed that the mean free path of an individual molecule depends on the direction of motion and may be infinite in some directions, while finite in all others. The conditions for escape of a molecule are: (1) The velocity must be sufficiently large not only to take the molecule out of the Earth's gravitational field, but also to avoid further collisions; (2) The direction of motion after the last collision must fall within a 'cone of escape', the size of which depends on the position of this collision. It is obvious that this cone, the axis of which is the upward vertical, will open out with height. At the critical level this cone degenerates into the vertical axis.

Spitzer (1949) noted that the critical level can be chosen as the height at which the mean free path for a particle moving in the horizontal direction equals the scale height. Öpik and Singer (1969) prefer for the critical level the height at which the number density is such that for an omnidirectional escape flux, the probability of collisions is $\frac{1}{2}$, i.e. the mean free path is approximately two times the scale height of the principal constituent. Although the latter definition is to be preferred, the choice of the exobase remains a matter of convention since in any planetary atmosphere the collision dominated region or *barosphere* is separated from the collisionfree exosphere by a narrow transition layer in which the collision frequency gradually decreases outwards. Introducing the concept of critical level is equivalent to assuming that this transition layer is reduced to a sharply defined surface, which offers a simple convenient method for estimating the rate of escape.

In the last two decades the study of the problem of escape from planetary atmospheres and the distribution of density in the exosphere has known a great revival. Öpik and Singer (1959, 1960, 1961) showed that the barometric formula cannot give the correct density distribution in the exosphere (see also Singer 1960a). Under the assumption that the exosphere is only populated by particles travelling upward from the barosphere and that these particles have a Maxwellian velocity distribution at the exobase, the partial number density of the ballistic re-entry component and the escaping particles were calculated separately. The former kind of particles which under the influence of the gravitation pull fall down into the barosphere are dominant at the critical level compared to the latter which have a hyperbolic trajectory and escape into interplanetary space. Quite similar results were obtained with different methods by Aamodt and Case (1962), Herring and Kyle (1961), Shen (1963), and Chamberlain (1963) who determined the 'ballistic' number density analytically (see also Goddard, 1963; Nicolet, 1964).

Brandt and Chamberlain (1960) stressed that the bound orbit components or satellite particles, whose orbits do not intersect the exobase, must be included for a complete description of the neutral exosphere, especially for the neutral hydrogen distribution in the Earth's atmosphere. Indeed, since in a real planetary exosphere some collisions will occur above the base of the exosphere there will always be ballistic particles which will be injected into trapped or satellite orbits. On the other hand, some of these satellite particles will in their turn be brought back into the ballistic class of particles. The trapped elliptic orbits will become depleted with increasing height (Chamberlain, 1963) and at several Earth radii it is not so clear whether or not the exosphere is populated by satellite hydrogen atoms (Johnson and Fish, 1960; Johnson, 1961). From recent Lα airglow observations there is some evidence that below a radial distance of 2.5 Earth's radii there would exist a complete isotropic distribution of trapped hydrogen atoms. Above this level the population of the satellite orbits seems to be negligible (Meier and Mange, 1970; Mange, 1972; Bertaux and Blamont, 1973). Moreover the effect of the rare collisions in the exosphere on the escaping particles has been considered by Fahr (1971) who calculated that the escape rate is reduced to about 90% of the value given by Jeans' formula. The importance of charge exchange

with solar wind protons and the influence of radiation pressure for the satellite particle distribution in the upper exosphere have been discussed by Bertaux and Blamont (1973).

All these investigations of the exosphere are based on the assumption that below the critical level, the atmosphere is isothermal and collision dominated, i.e. the velocity distribution in the barosphere and even at the escape level is supposed to be a Maxwell-Boltzmann distribution function. However, the process of escape would destroy the equilibrium velocity distribution of particles in the atmosphere (Pikel'ner, 1951). Therefore escape rates based on the formula of Jeans represent only upper limits of the actual dissipation, since the high-energy tail of the distribution becomes depopulated. As a consequence of this process, called 'anisotropic cooling', both the temperature and the temperature gradient vary with direction (Liwshitz and Singer, 1966; Liwshitz, 1967).

Analytic approaches to the calculation of the departure of the velocity distribution from the equilibrium form were given by Biutner (1958, 1959), Chamberlain (1963), and Hays and Liu (1965). Biutner and Chamberlain concentrated their investigations on the high energy-tail and concluded that the inclusion of the effects of cooling due to the escape process cannot change the order of magnitude of escape (a reduction of 20–50% compared to Jeans' formula for most cases of practical interest). Hays and Liu's analysis based upon an integral formulation of the Boltzmann equation showed that the reduction of escape flux is large when the background gas is heavy compared to the escaping gas, but that this reduction would be negligible when the escaping gas and the background gas have equal molecular weight.

On the other hand, the problem has been attacked by statistical sampling technics (Brinkmann, 1970, 1971; Chamberlain, 1969; Chamberlain and Campbell, 1967; Chamberlain and Smith, 1971; Lew, 1967; Lew and Venkateswaran, 1965, 1966; Liwshitz, 1966; Liwshitz and Singer, 1966; Venkateswaran, 1971). All the results derived prior to 1970 should be regarded with suspicion because of inadequacies in the physical models employed (Brinkmann, 1971). According to Brinkmann (1970) the escape fluxes of hydrogen and helium from the Earth's atmosphere are 70–75% and 97–99% of Jeans' escape fluxes respectively.

Most of the exospheric models neglect the planetary rotation. The evaporative loss from rotating planets was studied by Bryan (1901), Hagenbuch and Hartle (1969), Burke (1969), and Hartle (1971). It is obvious that particles with thermal velocities in the same direction as the rotational motion of the planet will more easily escape than those with thermal velocities in the opposite direction. According to Burke (1969), simply regarding the rotation as diminishing the gravity pull may underestimate the escape rate since evaporation from a rotating planet is not only selective in that it preferentially removes the most energetic particles at the critical level, but is additionally selective in removing particles of greatest forward angular momentum. Moreover, when rotation is taken into account, the number density and radial flux are for a fixed radial distance monotonic decreasing functions of the latitude, i.e. the rate of escape at the equator will exceed that at the poles. Hagenbuch and Hartle (1969)

showed that the effects of rotation are small for hydrogen but become much more important for heavier constituents.

The previous exospheric models which were developed under the assumption that the number density and the temperature at the exobase are constants lead to a spherical symmetric exospheric density distribution if rotation is neglected. The hydrogen escape is however so highly temperature dependent that the hydrogen concentration in the steady state is much larger on the night side than on the dayside. The effect of a nonuniform exobase, i.e. an exobase with lateral temperature and density gradients, has been studied by several authors (Hanson and Patterson, 1963; Donahue and McAfee, 1964; Patterson, 1966; McAfee, 1965, 1967; Hodges and Johnson, 1968; Fahr, 1970; Hartle, 1971, Vidal-Madjar and Bertaux, 1972; Quessette, 1972). The ballistic re-entry trajectories carry atoms from one point of the exobase to an other point with different temperature and density conditions. Therefore the flux at the exobase is not only determined by the escaping particles. The net upward flux of the non escaping particles at the exobase determines the lateral flow through the exosphere. There will be a net flow from the point of larger concentrations to the point of smaller concentrations, and from the high temperature point to the low temperature point. This would tend to lessen the flows and the atmosphere would tend toward a situation in which there is no net lateral flux. McAfee (1967) calculated that the distributions in concentration necessary for a zero flux situation show about a 2 to 1 diurnal variation.

2.2. The ion-exosphere

Mitra and Banerjee (1939) pointed out that the escape of neutral particles in the exosphere will also be influenced by the possibility of ionization and Öpik (1963) calculated the escape flux of charged particles in the absence of a magnetic field. The dynamical behavior and the number density distribution of the electrons and the ions in the terrestrial atmosphere however will be greatly influenced by the geomagnetic field. Nowadays, it is well accepted that the geomagnetic field lines intersecting the earth surface at the polar regions are open (Ness, 1965) whereas the low- and mid-latitude geomagnetic field can be approximated fairly well by a centered dipole magnetic field (Roederer, 1969). Therefore the ions and electrons in the low- and mid-latitude ionosphere spiraling around the convecting magnetic field lines, will be confined to the vicinity of the Earth and the ion-electron plasma will partake of the Earth's rotation (Hones and Bergson, 1965) whereas the neutral particles in the exosphere do not maintain their angular velocity. The ionospheric plasma in the polar regions, however, can escape into the geomagnetic tail (Dungey, 1961, 1967; Bauer, 1966; Dessler and Michel, 1966; Nishida, 1966).

Since the Coulomb cross-section is much larger than the gas-kinetic cross section, the critical level for charged particles will be much higher than the escape level for the neutral constituents of the atmosphere. The number densities of the ions and the electrons in the neutral exosphere (i.e. in the region above the exobase for the neutrals but below the critical level for the charged particles) have been calculated by several authors (see e.g. Johnson, 1960a, b; Bates and Patterson, 1961; Angerami and Thomas,

1964; Colin and Dufour, 1968; Mayr *et al.*, 1972; Moffet and Hanson, 1973). Under the assumption of diffusive equilibrium Mange (1960) and Gliddon (1963) determined the electric field in the ionosphere which arises due to the small charge separation between the electrons and the heavier ions. This electric field tends to reduce the 'weight' of the ions and also tends to restrain the electrons from rising. In the case of two constituents the reduction of weight of the ions is approximatively given by $T_{\text{ion}}/(T_{\text{ion}}+T_e)$ where T_e and T_{ion} are the electron and ion temperature, respectively (Singer, 1960; Kamiyama, 1968). For $T_e=T_{\text{ion}}$, this charge separation electric field is reduced to the wellknown Pannekoek (1922)-Rosseland (1924) electric field.

Studies of the ion-exosphere (i.e. the region above the critical level for the charged particles) are rather scarce. Eviatar *et al.* (1964) calculated the number density distribution of the ions and electrons for a non-rotating planet with a dipole magnetic field under the assumptions that these particles were moving without collisions under the influence of the gravitational pull and the charge separation electric field. The dynamical behavior of the charged particles was described by means of the guiding center approximation and the drift across magnetic field lines was neglected so that the number density distributions along different lines of force are independent of each other. They considered a two-constituent ionosphere in which the 'trapped' particles (i.e. particles with two mirror points in the exosphere itself) are missing. The transition region between the collision dominated and the collision free regions was reduced to a surface discontinuity and the particle density and temperature at the exobase were assumed to be uniform. The charge separation electric field is then given by the Pannekoek-Rosseland field which yields the quasi-neutrality everywhere in the exosphere. The same electric field was used for the model ion-exosphere of Hartle (1969) who generalized the calculations of Eviatar *et al.* (1964) by assuming that the density and temperature are allowed to vary over the baropause which is symmetric about the magnetic equator but need not to be spherical symmetric. In particular, the density and/or temperature are allowed to differ at the conjugate magnetic field points of the baropause. Kamiyama and Takaki (1966) considered the case in which the ion-exosphere, located above 3000 km altitude, rotates around the dipole axis. They deduced exospheric ion densities by estimating the time during which an ion travels a unit length along the field line.

Since a dipole magnetic field was assumed for these ion-exospheres they only can be applied to the low- and mid-latitude regions of the earth. In the high-latitude regions, where the magnetic field lines are open, the escape energy for the ions will be smaller than for the corresponding neutral atoms as a consequence of the polarization electric field induced in the ionosphere by gravitational and thermal charge separation. Lemaire and Scherer (1969) have shown that in an open ion-exosphere this electric field is no longer given by the Pannekoek-Rosseland field since this would lead to a larger efflux for the electrons than for the ions. A continuous positive charge deposition would result at the baropause and consequently the outward directed electric field in the exosphere would increase until a stationary state is reached in which the flux of the electrons is equal to the flux of the positive ions.

The escape of ionized hydrogen by means of an evaporative process similar to the evaporation of neutral hydrogen was discussed by Dessler and Michel (1966) who also estimated the number density of the evaporated plasma in the geomagnetic tail. According to Axford (1968) the lighter ions in the polar ionosphere must be dragged away from the Earth by the escaping photoelectron flux and the resulting ion flow would become rapidly supersonic. By analogy of the solar wind phenomenon, Axford called this outward flowing ionospheric plasma the *polar wind.* Several years before, Nicolet (1961) noted that the thermal escape of neutral helium cannot support the large He^4 production, and since the photoionization rate of He^4 is almost equal to its production rate, he put forward the idea that terrestrial helium possibly escapes in its ionized state. Banks and Holzer (1968) described the polar wind by means of Euler's hydrodynamic equations for an isothermal temperature distribution. The oxygen and helium ions are produced by photoionization, whereas the hydrogen ions are created by charge transfer between O^+ and H. The electronic pressure gradient yields an electric field which accelerates the ions outwards and decelerates the escaping electrons. To calculate the flow speeds Banks and Holzer (1968) chose the supersonic solution which passes through a critical point and which yields a nearly zero plasma pressure at large radial distances.

The hydrodynamic description of Banks and Holzer was seriously questioned by Dessler and Cloutier (1969) who argued that most of the acceleration of the light ions takes place in the ion-exosphere and is due to the small gravitational charge separation electric field (which they assumed to be the wellknown Pannekoek-Rosseland field in an O^+ ionosphere) and not to the partial pressure gradient of the ion gas. As counter part to the hydrodynamic approach they proposed a single particle evaporative *polar breeze* model in which collisions are neglected beyond the exobase. For a discussion of this controversy we refer to the review papers by Donahue (1971) and Lemaire and Scherer (1973a).

The applicability of the hydrodynamic approximation to the ion-escape problem has also been considered by Marubashi (1970a) and the mathematical difficulties inherent in the existence of singularities at the critical points of the hydrodynamic polar wind equations are discussed in detail by Strobel and Weber (1972). Marubashi (1970a) showed that an effective collision frequency about 10 times larger than the classical Coulomb collision is required for the hydrodynamic approach to be valid throughout the upper ionosphere; he also discussed the possibility of an evaporative approach to the polar ion-escape.

The kinetic approach introduced by Dessler and Cloutier (1969) was modified by Lemaire and Scherer (1969, 1970, 1971, 1972a) who considered a three component (O^+, H^+, e) polar ionospheric model for which the charge separation electric field is calculated by using the quasi-neutrality condition and the zero-electric current condition everywhere in the exosphere. By the combined effect of the gravitational pull and the induced electric field the ionospheric electrons and oxygen ions are decelerated whereas the ionospheric hydrogen ions are accelerated outward and reach supersonic flow speeds which tend to a constant value (≈ 20 km s^{-1}) at large radial distances.

This kinetic approach yielded a much more realistic oxygen ion escape flux several orders of magnitude smaller than the O^+ flux obtained in the original polar wind model of Banks and Holzer (1968). Although Banks and Holzer (1969a, b, c) reduced the oxygen flow in subsequent models, they still obtain too large values. In Marubashi's (1970a) hydrodynamic model the oxygen ions are in hydrostatic equilibrium, (i.e. the oxygen ion escape flux is zero) which seems to be a good approximation.

Since the model calculations of Banks and Holzer (1969a, b, c) and Marubashi (1970a) showed that the critical point of the hydrodynamic theory lies in the collision-free exosphere, Lemaire (1972a) proposed to match the hydrodynamic solution to the kinetic solution in the subsonic region, i.e. below the critical point. Instead of requiring that the hydrodynamic solution passes through the critical point he chose that solution of the hydrodynamic polar wind equations which gives at the exobase a diffusion flux equal to the escape flux calculated by means of the kinetic method of Lemaire and Scherer. Therefore the hydrodynamic and kinetic approaches are not at all contradictory but complementary (see Mange, 1972). The hydrodynamic treatment developed by Banks and Holzer (1968, 1969a, b, c) and Marubashi (1970a) is appropriate in the collision dominated region below the ion-exobase, whereas the kinetic approach introduced by Dessler and Cloutier (1969) and modified by Lemaire and Scherer (1969, 1970, 1971, 1972a) is only valid in the collision-free ion-exosphere.

A collisionless strongly magnetized plasma can also be described by the CGL hydromagnetic equations established by Chew, Goldberger, and Low (1956) and extended by Macmahon (1965). Holzer *et al.* (1971) calculated collisionless polar wind models in a CGL approximation. Although they called this an 'extended hydrodynamic description', the *CGL hydromagnetic* and the *classical hydrodynamic* formulations are physically different approximations of the general transport equations. The latter cannot describe in a fully satisfactory manner the collisionless region and the former, which supports a comparison with the kinetic formulation cannot correctly describe plasma flow in the collision-dominated region (see Lemaire and Scherer, 1973a). Holzer *et al.* (1971) also considered a *semi-kinetic* polar wind model in which only the protons are collision-free while the electron gas behaves as an isothermal fluid throughout the ion-exosphere. They showed that the number densities and flow speeds calculated with the CGL hydromagnetic equations are in quite good agreement with the results obtained by the semi-kinetic formulation when the same boundary conditions are used at a reference level where the Coulomb mean free path is larger than the electron density scale height, and where the flow speed is already supersonic.

All these model calculations show that a continuous plasma escape can take place in the polar regions, even in the winter polar ionosphere where no photoelectron flux is present. Kinetic polar wind models for the sunlit atmosphere where the photoelectrons yield an additional electric drag, have shown that the escape flux, the flow speed, and the parallel and perpendicular temperatures of the thermal electrons are strongly dependent on the value of the photoelectron efflux, while the number densities of the ionized hydrogen and oxygen remain practically unchanged (Lemaire, 1972b; Lemaire and Scherer, 1972b).

Moreover it is worthwhile to mention that recent studies (Lemaire and Scherer, 1973b; Knight, 1973) have shown that the kinetic approach is very useful in the discussion of plasmasheet particle precipitation along auroral field lines. Besides the thermal electrons and ions, the presence of different suprathermal particles and field aligned currents can be taken into account in kinetic model calculations.

Several indirect evidences of the polar wind have been reviewed by Marubashi (1970b), Banks (1971), and Mange (1972). Direct measurements of upward ionized hydrogen and helium fluxes were obtained by Hofmann (1968, 1970, 1972) with Explorer 31. From these results it follows that, at 3000 km altitude, H^+ is the principal constituent and O^+ is not observed at mid- and low-altitudes, but in the polar upper ionosphere ionized oxygen becomes dominant as a consequence of the large escape flux of H^+ streaming with supersonic velocities of 10 to 15 km s^{-1}. Large amounts of ion and electron densities and temperatures in the topside ionosphere have been provided by recent satellite measurements (see e.g. Brace *et al.*, 1967, 1970; Brinton *et al.*, 1971; Taylor, 1971a, b, 1972; Taylor *et al.*, 1965, 1968, 1969; Thomas *et al.*, 1966; Tulunay, 1972, 1973; Tulunay *et al.*, 1971, 1973). Moreover the extension of the ionosphere into the magnetosphere has been investigated by whistler technics and by in situ satellite measurements. The results are reviewed by Carpenter and Park (1973) and by Chappell (1972).

3. The Ionospheric Regions

The ionosphere is usually divided into horizontal layers (D, E, F, Heliosphere, Protonosphere) according to the relative importance of the different photo-chemical and physical processes responsible for production and maintenance of ionization in the Earth's atmosphere. Figure 1 shows this well-known division into layers with a low latitude electron density profile, n_e (solid line), and a neutral density distribution, n_N for $T_N = 1500$ K (dashed line). The order of magnitude of some characteristic lengths (l_e: the electron mean free path; H_e: the electron density scale height; $r_{L.e}$: the Larmor radius of a thermal electron) at some typical altitudes are also reported in the right hand side panel of Figure 1.

Since in the D-region the value of the mean free path of the electrons is comparable to the Larmor radius, the electric conductivity coefficient is nearly isotropic with respect to the magnetic field direction. Above the D-region the mean free path becomes much larger than the Larmor radius, and the electric conductivity coefficient of the partially ionized gas becomes highly anisotropic with respect to the geomagnetic field direction. Above 400–600 km, the geomagnetic field completely controls the dynamics and the distribution of the ambient ions and electrons. Since the magnetospheric structure varies with latitude, the topside ionization distribution will also depend on the latitude. Figure 2 (from Taylor, 1971a) illustrates this latitudinal dependence of the hydrogen and oxygen ions along the OGO 6 orbit during quiet time conditions. Characteristic differences between the high-latitude and low-latitude topside ionosphere are also illustrated in the Table on the right hand side of Figure 1 where the numbers between parentheses correspond to a high-latitude region and those without

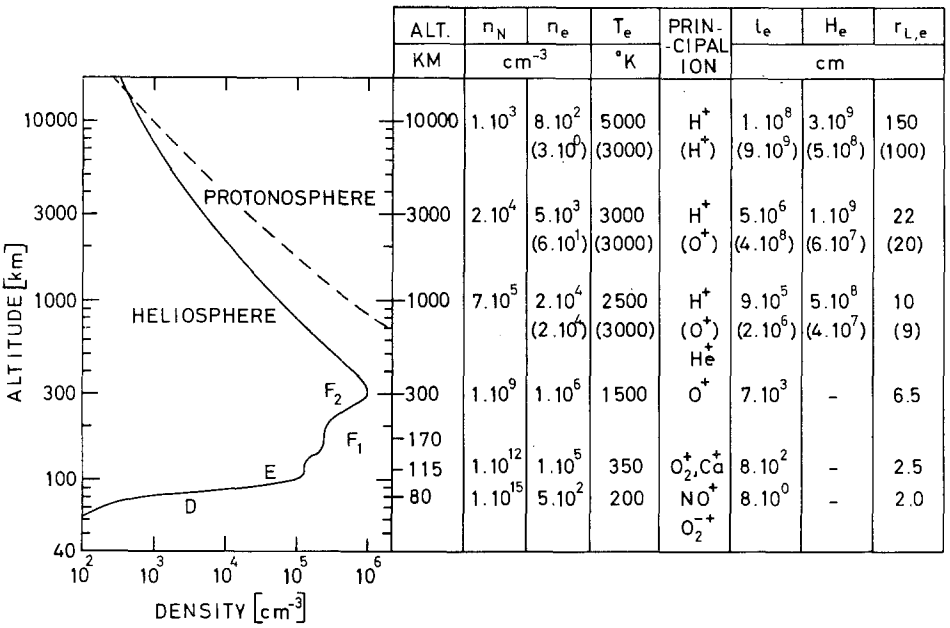

Fig. 1. *Ionospheric layers.* The solid line is a typical electron density profile (n_e) of the low-latitude ionosphere. The dashed line is the neutral density (n_N) corresponding to a thermospheric temperature $T_N = 1500$K (Nicolet and Kockarts, personal communication, 1971). The electron temperature (T_e), mean free path (l_e), scale height (H_e), and mean Larmor radius ($r_{L,e}$) are given at the right hand side for some typical altitudes in the low-latitude ionosphere (numbers without parentheses) and in the high-latitude ionosphere (numbers with parentheses).

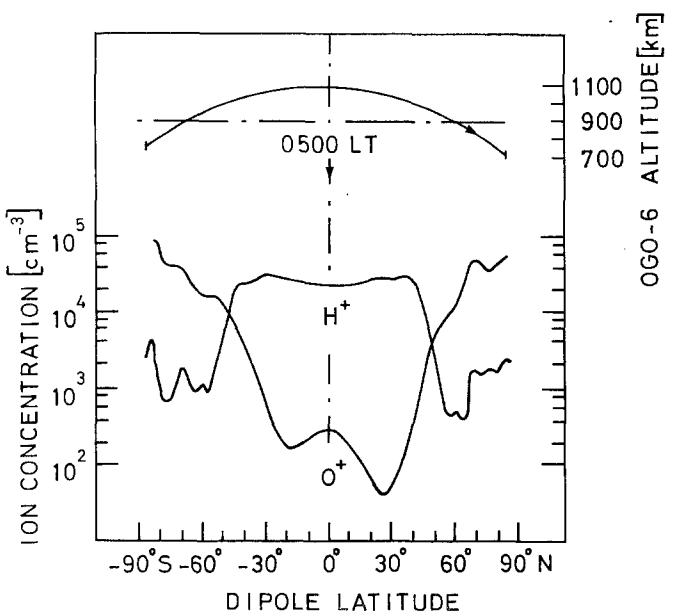

Fig. 2. *Latitudinal variation of* H^+ *and* O^+ *ion concentrations in the topside ionosphere.* These data are obtained from OGO 6 ion mass spectrometer measurements made on September 23, 1969, when the K_p index was lower than 0_+, and when the tilt angle was small ($\alpha = 7°$) and consistent with nearly symmetrical equinox conditions. The latitude of the OGO 6 polar satellite, orbiting in the dawn side, is given at the top. (From Taylor, 1971a.)

parentheses to a low-latitude region. It can for instance be seen that the ionization density, n_e, decreases much more rapidly with altitude along high-latitude field lines than in the low-latitude ionosphere. Therefore the electron density scale height is smaller and the mean free path is larger in the polar topside ionosphere than in the equatorial upper regions.

By analogy of the neutral exosphere the ion-exobase is defined as the critical level where the mean free path of the charged particles in a horizontal direction equals the scale height for the ionized gas:

$$l = H_e. \tag{1}$$

From the table in Figure 1, it can be seen that the ion-exosphere is located between 1000 and 1500 km in the high latitude regions. At low latitudes ($\lambda < 60°$, $L < 4$–5) the mean free path of a thermal electron along a closed field line remains smaller than the electron density scale height. Therefore at low-latitudes the collision-dominated region coincides with the plasmasphere. Indeed, at an equatorial distance of $4R_E (L=4)$ whistler observations (Carpenter, 1966, 1970; Carpenter and Park, 1973) and in situ satellite measurements (Chappell *et al.*, 1970a, b, 1971; Chappell, 1972) revealed that the electron and ion density is at least equal to 10^2 cm^{-3}. Serbu and Maier (1966, 1970) have shown that the electron temperature at these large radial distances is of the order of 10^4 K. Hence the electron mean free path

$$l_e \approx 3 \times 10^3 \frac{T_e^2}{n_e} \quad \text{(cm)} \tag{2}$$

(Spitzer, 1956; T_e in °K and n_e in cm^{-3}) is approximately 30000 km. On the other hand the length of the magnetic field line $L=4$, is equal to 24000 km. Furthermore l_e is much smaller than the local density scale height, and consequently the electrons are collision-dominated in the whole plasmasphere.

Beyond the plasmasphere the electron density decreases to a value of 1 cm^{-3} (Carpenter and Park, 1973; Chappell, 1972), and the mean free path which increases by two orders of magnitude ($l = 3 \times 10^6$ km), becomes larger than the length of the magnetic field line. Therefore the ion-exobase in the low-latitude region coincides with the knee or plasmapause surface. The solid line separating the shaded and unshaded regions in Figure 3 illustrates the position of the ion-exobase as a function of latitude.

This paper is mainly devoted to the kinetic approach and therefore we will not discuss the collision-dominated region, but confine ourselves to the high-latitude and trough regions of the ion-exosphere. Inside the plasmasphere and below the ion-exobase the hydrostatic models reviewed by Bauer (1969), or the hydrodynamic models studied by Mayr *et al.* (1972) are quite appropriated as a consequence of the large collision rate. In the collisionless region beyond the plasmapause and above the exobase, a kinetic theory based on Liouville's equation is more justified than the classical

hydrodynamic theory based on Euler's or Navier-Stokes transport equations. Indeed the latter approximations were established for dynamical or static situations where the mean free path is much smaller than the length characterizing the dimension of the system (i.e. the density or temperature scale height, or the distance separating the 'walls', which in the present case corresponds to the length of the magnetic field lines).

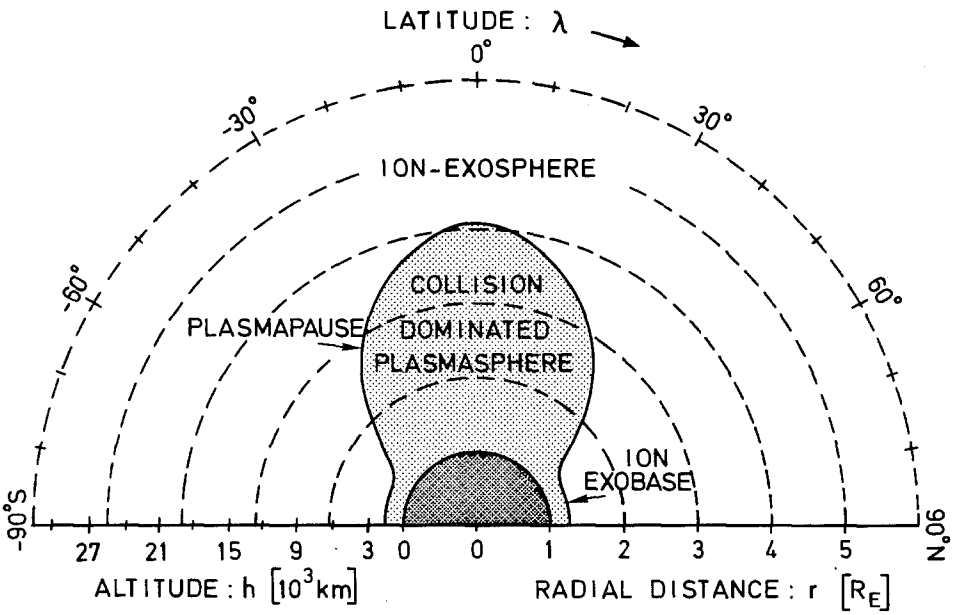

Fig. 3. The collision-dominated region (shaded area) and collisionless ion-exosphere (unshaded area) separated by the ion-exobase which coïncides with the plasmapause in the low latitude region.

Evidence for the validity of a kinetic description is also obtained from the observed r^{-4} electron density variation beyond the plasmapause (Carpenter and Park, 1973; Chappell, 1972). Indeed in Section 5.5 it will be shown that kinetic or exospheric models can account of such a rapid density decrease, while diffusive equilibrium or hydrostatic models would predict much to large equatorial densities beyond the knee or plasmapause.

4. The Kinetic Description

As shown in the Section 2.1, the kinetic theory has been used many times to determine the escape flux of the neutral atoms from the Earth's atmosphere. An analogous method can be developed for ions and electrons whose mean free path (for Coulomb collisions with impact parameters smaller than the Debye length) is larger than the characteristic dimension of the system. There are however some major differences between the exospheric theories for neutral atmospheres on the one hand, and charged particles on the other hand.

4.1. Comparison between neutral and ion-exosphere theories

(1) While neutral exospheric particles orbit around the Earth on elliptic, parabolic or hyperbolic trajectories as a consequence of the total energy and angular momentum conservation, the charged particles have helicoidal paths along the magnetic field lines as a consequence of energy and magnetic moment conservation. It can be shown that only in the case of a monopole (or radial) magnetic field configuration the angular momentum and magnetic moment conservation lead to a similar classification in velocity space. For any other magnetic field configuration (e.g. a dipole) the classification of particle orbits will be different (see Appendix A).

In a dipole magnetic field the charged particles emerging from the ionosphere may have enough kinetic energy and a sufficiently small pitch angle to reach the equatorial plane; they will be called *escaping* particles. In the polar ion-exosphere the escaping particles are those which can reach 'infinity' along open field lines. On the other hand the particles may have enough kinetic energy to escape into the other hemisphere but a too large pitch angle to reach the equatorial plane. In this case they are reflected magnetically and fall back toward the ionosphere in the same hemisphere, they belong to the class of *ballistic* particles. Particles with a kinetic energy smaller than the escape energy necessary to overcome the potential barrier between the exobase and the equator are gravitationally or magnetically reflected and they belong also to the ballistic particles. Other types of orbits correspond to *trapped* trajectories with reflection points located above the ion-exobase. These mirror points can both be located in the same hemisphere or are in different hemispheres. The velocity distribution of such particles in collisionless models can be chosen arbitrarily. Mostly the trapped particles are assumed to be missing. Finally there are the so called *incoming* particles which come from the conjugate ionosphere or are injected at the equatorial plane with pitch angles inside the loss cone. This classification was first described for closed field lines by Eviatar *et al.* (1964) and was extended by Lemaire and Scherer (1970, 1971) for open field lines.

(2) A second important difference between neutral exospheres and ion-exospheres is that in the latter electric fields play an important role on the dynamical behavior of the particles. The corotational and magnetospheric convection electric fields are perpendicular to the magnetic field direction (Hones and Bergeson, 1965; Axford and Hines, 1961; Dungey, 1961) and do not directly influence the motion of particles along the field line. Their indirect effect will be discussed in Section 5.3.

The parallel electric fields which are charge separation or polarization electric fields play however a primary role in the ion-exosphere. In the magneto-hydrodynamic (MHD) theory it is assumed that the electric conductivity parallel to the magnetic field direction, is so large that the parallel electric field intensity must be nearly zero. However, due to the finiteness of the electron mobility this approximation ($E_{\parallel}=0$) may in certain circumstances lead to ion density distributions which are not balanced by the electron density as it should be to maintain the local quasi-neutrality in a plasma.

For example, a plasma sustained in hydrostatic and isothermal equilibrium in a

gravitational field will become polarized due to the tendency of gravitational charge separation of the electrons and heavier ions. The resultant vertical electric field, **E**, experienced by the charges inside this plasma is given by the Pannekoek (1922)-Rosseland (1924) formula

$$\mathbf{E} = -\frac{m_+ - m_e}{2e}\mathbf{g}, \tag{3}$$

where m_e and m_+ are respectively the electron and mean ion masses, e is the electronic charge, and **g** is the gravitational acceleration. In the ionosphere this corresponds to a small upward directed field of $5\text{–}80 \times 10^{-5}$ mV m^{-1} depending on the value of the mean ion mass m_+. In the Vlasov equation for a collisionless plasma this electric field which is the result of collective long range interactions (i.e. Coulomb collisions with impact parameters larger than the Debye length) tends to zero when there are no external gravitational nor centrifugal forces, and no electron pressure gradients in the direction of the magnetic field.

Along closed field lines and for plasma densities and temperatures strictly symmetric about the magnetic equator the Pannekoek-Rosseland electric field established for a collision-dominated plasma in hydrostatic equilibrium is still appropriated in a two constituent ion-exosphere since there are no interhemispheric charge fluxes and the local quasi-neutrality is maintained.

In the polar ion-exosphere where the field lines are open or extend far into the magnetotail, the electrons have a tendency to fill more rapidly the outer space than the heavier ions. Consequently, in the absence of field aligned currents a thermal charge separation electric field will be set up to reduce the electron efflux F_e, and to make it equal to the total ion escape flux $\Sigma_i F_i$. In the presence of a parallel electric current $j_\parallel$, however, the electric field in the ion-exosphere must be adjusted to satisfy the condition

$$j_\parallel = e(\Sigma_i F_i - F_e). \tag{4}$$

This equation determines the electric potential difference between the baropause and the equatorial plane (Lemaire and Scherer, 1973b; Knight, 1973). The detailed structure of the parallel electric field distribution $E_\parallel$ can be determined in order to match the electron density n_e to the total ion density $\Sigma_i n_i$ everywhere in the exosphere. This is obtained by solving the equation

$$n_e(\mathbf{r}) = \Sigma_i n_i(\mathbf{r}). \tag{5}$$

(3) A third important difference between the kinetic theories for neutral and ionized exospheres is that in the latter the boundary conditions need only to be specified at the ends of the field lines, while in the neutral case the exobase density and temperature distributions must in principal be known over the globe (see Section 2.1).

4.2. Comparison to the CGL formulation

Besides the kinetic formulation described in this paper, there is a physically equivalent but formally different method which can be used to describe the ion-exosphere. This

is the CGL approximation originally developed by Chew, Goldberger, and Low (1956). The CGL equations are macroscopic transport equations obtained from the collisionless Boltzmann or Vlasov equation. To close this unlimited set of differential equations some convenient assumptions are made about the velocity distribution $f(\mathbf{v})$ or, equivalently, about a predetermined number of moments, of this distribution. These moments are related to the number density n, the flux of particles F, the pressure tensor components $p_{\parallel}$ and $p_{\perp}$, the energy flux tensor $\mathbf{q}$, etc. The necessary assumptions to be made for the velocity distribution (degree of asymmetry, anisotropy, and skewness) are suggested by the type of velocity distribution observed at a given point or reference level in the collisionless medium. It is equivalent to specify appropriate expressions of the higher order moments $(p_{\parallel}, p_{\perp}, q_{\parallel}, q_{\perp}, \ldots)$ in terms of the lower order macroscopic variables. When the value of these macroscopic quantities are determined at some reference level, it is possible to integrate the closed set of differential equations and obtain numerical values of all the predetermined moments, at any other point in the ion-exosphere.

In the kinetic theory the collisionless Boltzmann or Vlasov equation is integrated directly. When the velocity distribution function is specified at a reference level (exobase) the velocity distribution can be obtained at any other point in the ion-exosphere in an analytic form (Aamodt and Case, 1962).

In the exospheric or kinetic theories $f_0(\mathbf{v}_0)$, the velocity distribution at the exobase, is usually assumed to be a truncated Maxwellian velocity distribution with no incoming particles (when the field lines are open). The choice of a maxwellian distribution at the exobase is usually justified in the older evaporative interpretation by the proximity of the collision-dominated region where the actual velocity distribution is thought to be nearly Maxwellian. In the new interpretation proposed by Lemaire (1972) $f_0(\mathbf{v}_0)$ is a convenient boundary condition for the Vlasov equation, and need not to be a realistic microscopic representation of the actual velocity distribution at the top of the collision-dominated region. It is always possible to build up an arbitrary function of the velocity, $f_0(\mathbf{v}_0; \boldsymbol{\sigma})$, such that the s first moments of this function coincide with the s corresponding moments of the actual velocity distribution at the exobase reference level. Although there are many ways to build such a function $f_0(\mathbf{v}_0; \boldsymbol{\sigma})$, a linear combination of truncated maxwellians is rather convenient since kinetic theories have usually been developed for maxwellian functions. A fixed number s of the parameters $\boldsymbol{\sigma}$ can be determined in order to avoid zero order discontinuities (jumps) across the exobase surface for the s first moments. As a consequence of the artificial discontinuity between the collision-dominated and collisionless regions, the first order or gradient discontinuities can not be avoided.

While in the CGL formulation the macroscopic variables $(n, F, \mathbf{p}, \mathbf{q}, \ldots)$ will satisfy a limited set of specific transport equations, the same variables when determined from the kinetic method, will satisfy the unlimited set of the original transport equations since they are deduced directly from the collisionless Boltzmann equation. Furthermore in the CGL approximation the differential equations to be solved will depend on the assumption made about the shape (asymmetry, anisotropy, and higher order skew-

ness) of the velocity distribution, and will become very cumbersome to handle when higher order moments fitting is required.

In the CGL formulation only the ions are described as collisionless while the electrons are treated as a collision-dominated fluid whose distribution along the field lines is given by

$$e\mathbf{E}_{\parallel} = -\frac{1}{n_e}\nabla_{\parallel} p_e , \tag{6}$$

where n_e and p_e are the electron density and pressure. As long as the electron pressure is not anisotropic this is a good approximation. In the kinetic formulation the electrons as well as the ions can be considered as collisionless, and a population of suprathermal particles can be added to the thermal ionization background, without further modification of the method. Comparisons of numerical results obtained by the two approaches are discussed elsewhere (Lemaire and Scherer, 1973a).

5. Collisionless Models for Closed Magnetic Field Lines

Feldstein and Starkov (1970) using the Alouette 2 data obtained the boundary of the stable trapping region of energetic electrons ($E > 35$ keV) which corresponds to the limit of the closed geomagnetic field lines. According to their results the equatorward boundary of the auroral oval is closely related to the position of the region in which the geomagnetic field lines change from closed to open. The geomagnetic latitude on the dayside is located at $\Lambda = 75°$–$78°$ depending on the orientation of the geomagnetic axis with respect to the streaming solar wind around the magnetosphere. Field lines with an invariant latitude Λ smaller than $75°$ or with a McIlwain parameter $L < 15$, link the particles from one hemisphere to the other.

In Section 3 it was shown that the Coulomb mean free path becomes larger than the length of the geomagnetic field line and also exceeds the electron density scale height beyond the trough latitude ($\Lambda_T = 50°$–$65°$) which corresponds approximately to the knee or plasmapause boundary ($L_p = 3$–6) (Rycroft and Thomas, 1970; Rycroft and Burnell, 1970; Taylor, 1972; Taylor and Walsh, 1972). The collisionless region along the closed field lines corresponding to L values between 3–6 and 10–15, will be described in the following paragraphs.

5.1. Symmetric collisionless models

Following Eviatar *et al.* (1964), we will first assume that the magnetic field is a centered dipole, and that the ionosphere does not rotate. It will also be assumed that the distributions of ionization at the ends of the fields lines are symmetric with respect to the magnetic equator, i.e. the ionosphere densities and temperatures are the same in both hemispheres. Under these symmetrical conditions there is no net interhemispheric ionization flow and the Pannekoek-Rosseland polarization electric field given by Equation (3), is appropriated to maintain the global and local quasi-neutrality in the collisionless medium. Indeed, the escape fluxes are equal in both hemispheres and there-

fore there will be as many incoming particles as there are escaping particles. As a consequence of the absence of collisions the trapped orbits are assumed to be empty.

For a maxwellian velocity distribution characterized by a density n_0 and a temperature T_0 at the critical level r_0 the exospheric number density at the latitude λ along a given field line L, is given by

$$n(\lambda; L) = n_0 \exp(-q)\left\{1 - (1-\eta)^{1/2} \exp\left[-\frac{\eta q}{1-\eta}\right]\right\}, \tag{7}$$

where η is the ratio of the magnetic field intensity $B(\lambda; L)$ to the field intensity at the exobase $B_0(\lambda_0; L)$. The variable η is also proportional to the inverse of the flux tube cross section. For a fully ionized hydrogen exosphere the reduced total potential energy of the charged particles is given by

$$q(\lambda; L) = -\frac{m_H^+ + m_e}{2} \frac{GM}{r_0 k T_0}\left[1 - \frac{r_0}{r}\right], \tag{8}$$

where G and k are respectively the gravitational constant and Boltzmann's constant; M is the mass of the Earth.

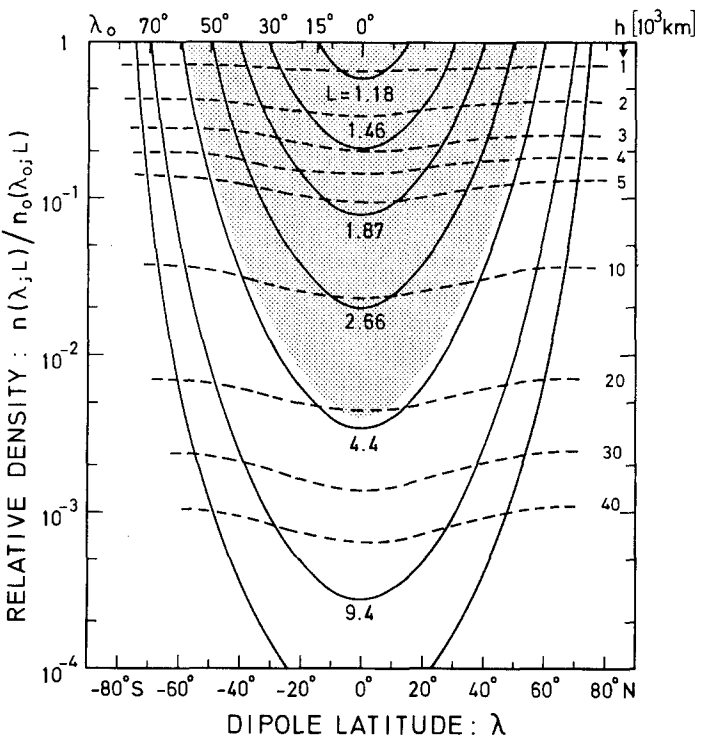

Fig. 4. *Relative density distribution in a symmetric non-rotating* (H^+, e) *ion-exosphere.* The solid lines give the distribution along different dipole field lines characterized by McIlwain's parameter L, and the exobase latitude λ_0. The exobase is taken at a radial distance $r_0 = 1.1\ R_E$, and the exobase electron and hydrogen ion temperatures are equal to 1500 K. The dashed lines give the latitudinal variation of the density at different constant altitude levels, h. The shaded area corresponds to the plasmasphere where collisionless models are not appropriate.

The solid curves in Figure 4 show the relative number density obtained as a function of latitude along different field lines. These results are deduced from Equation (7) for equal electron and hydrogen ion temperatures ($T_0 = 1500$ K) at the exobase located at a radial distance $r_0 = 1.1\ R_E$ (i.e. at an altitude $h_0 = 637$ km). The dashed lines illustrate the latitudinal density variation at different constant altitudes h, when the exobase boundary conditions are assumed to be uniform, i.e. independent of the latitude λ_0.

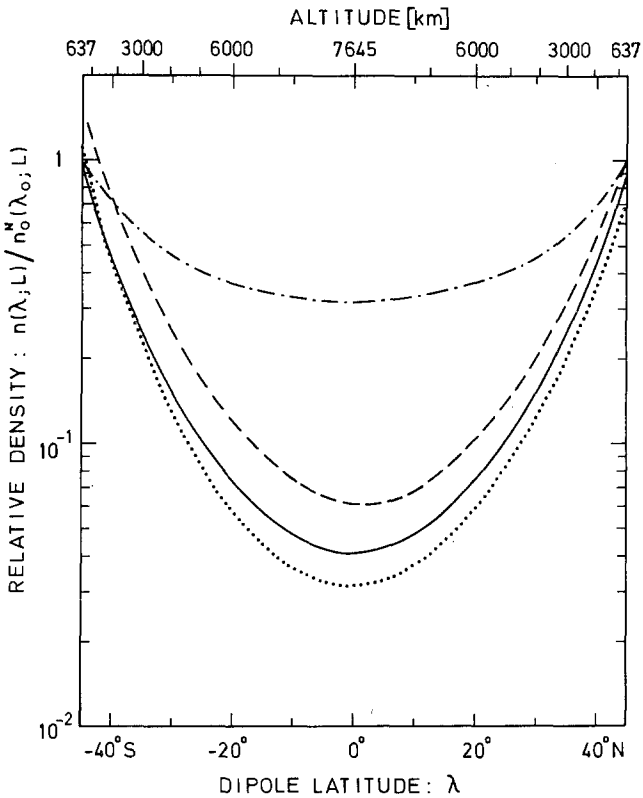

Fig. 5. *Barometric and collisionless density distributions in symmetric and asymmetric non-rotating* (H^+,e) *ion-exosphere models.* The dot-dashed line corresponds to the relative density distribution along the line of force $L = 2.2$ in a barometric or diffusive equilibrium model for a temperature $T_0 = 1500$ K at $\lambda_0 = \pm 45°$. The solid line corresponds to the relative density in Eviatar *et al.*'s (1964) collisionless model, with equal exobase temperatures in both hemispheres ($T_0 = 1500$ K at $\lambda_0 = \pm 45°$). The asymmetric models of Hartle (1969) are shown by the dashed line ($T_0^N = T_0^S = 1500$ K, $n_0^N/n_0^S = 0.5$) and the dotted line ($T_0^N = 1500$ K, $T_0^S = 750$ K, $n_0^N/n_0^S = 1$).

The equatorward decrease of the density at constant altitude is the result of the constraint for the charged particles to move along non-radial magnetic field lines (Eviatar *et al.*, 1964). Note that in the shaded region corresponding to the plasmasphere, the validity of collisionless models breaks down for the reasons discussed in Section 3.

The solid line in Figure 5 illustrates the collisionless density distribution along the field line $L = 2.2$ which intersects the exobase at the latitude $\lambda_0 = \pm 45°$. For comparison,

the dot-dashed line shows the barometric density distribution corresponding to the collision dominated or diffusive equilibrium case. The difference between the dot-dashed line and the solid line, corresponds to the relative amount of trapped particles in the barometric density distribution. It can be seen that the particles with high altitude mirror points have a vanishingly contribution near the exobase but that in the equatorial plane their density is almost equal to the total density. Hence it can be concluded that if the *plasmasphere* is well represented by a diffusion equilibrium model (as illustrated by the dot-dashed line), the trapped particles will give the major contribution to the total density.

5.2. Asymmetric collisionless models

Hartle (1969) generalized Eviatar *et al.*'s collisionless model calculations, by considering non-symmetric exobase conditions. In particular the density and/or temperature are assumed to be different at the conjugate magnetic field points of the baropause:

$$n_0^{\mathrm{N}}(\lambda_0, L) \neq n_0^{\mathrm{S}}(-\lambda_0, L)$$
$$T_0^{\mathrm{N}}(\lambda_0, L) \neq T_0^{\mathrm{S}}(-\lambda_0, L).$$

The dotted line in Figure 5 shows the relative density distribution $n(\lambda; L)/n_0^{\mathrm{N}}(\lambda_0; L)$ when the southern exobase temperature is reduced by a factor two compared to the northern exobase temperature: $T_0^{\mathrm{N}} = 1500\,\mathrm{K}$ and $T_0^{\mathrm{S}} = 750\,\mathrm{K}$. Due to the reduction of the particle injection rate in the southern hemisphere the total number of particles in the system is reduced. The decrease in the temperature at $\lambda_0 = 45°$, leads to a decrease in the high-energy tail of the velocity distribution of emerging particles and an increase in the number of low energy particles. Therefore, the relative number density just above the southern exobase is slightly enhanced, whereas at higher altitudes it is decreased. As a consequence of the reduction of the number of particles in the high-energy tail of the velocity distribution at the southern exobase, fewer particles are able to pass the equatorial potential barrier, and a larger reduction of the number density results in the northern hemisphere (Hartle, 1969). The dashed line in Figure 5 shows the relative density distribution under the assumption that the exobase temperature is 1500 K in both hemispheres but that $n_0^{\mathrm{S}} = 2n_0^{\mathrm{N}}$. The result is an overall increase of the relative density which can be explained by the increase in the particle injection rate into the ion-exosphere.

In both asymmetric situations, there will be an interhemispheric particle flux along the field lines from the hotter to the colder region and from the dense to the less denser ionosphere. The net flux of particles from the northern to the southern hemisphere is given by Hartle (1964):

$$F(\lambda; L) = \gamma n_0^N \left(\frac{kT_0^N}{2\pi m}\right)^{1/2} \exp(-\phi^N) \cdot \left[1 - (1-a)\exp\left(-\frac{a\phi^N}{1-a}\right)\right] +$$
$$- \gamma n_0^{\mathrm{S}} \left(\frac{kT_0^{\mathrm{S}}}{2\pi m}\right)^{1/2} \exp(-\phi^{\mathrm{S}}) \cdot \left[1 - (1-a)\exp\left(-\frac{a\phi^{\mathrm{S}}}{1-a}\right)\right], \qquad (9)$$

where

$$\gamma = \frac{B(\lambda; L)}{B_{eq}(0; L)}; \qquad a = \frac{B_{eq}(0; L)}{B_0(\lambda_0; L)}$$

$$\phi^{N,S} = -\frac{m_{H^+} + m_e}{2} \frac{GM}{r_0 k T_0^{N,S}} [1 - \cos^2 \lambda_0].$$

When there is a net particle flux ($F \neq 0$), a field aligned electric current will generally flow from one hemisphere into the other. These currents are often called Birkeland currents and are given by

$$j_{\parallel}(\lambda; L) = e(F_{H^+} - F_e). \tag{10}$$

In the present dynamical models with stationary and asymmetric boundary conditions, the polarization electric field can not be given by the Pannekoek-Rosseland formula (3) on which Hartle's calculations (dotted and dashed lines in Figure 5) are based. Indeed this electric field is only valid for a plasma in static isothermal equilibrium as for instance it is the case in Eviatar *et al.*'s (1964) model where the interhemispheric fluxes and current vanish because $n_0^N = n_0^S$ and $T_0^N = T_0^S$. In the asymmetric models considered by Hartle (1969), the flux $F(\lambda, L)$ for each kind of particles will vanish with the current $j_{\parallel}$, when the exobase conditions at both ends of the field lines satisfy the constraint

$$\frac{n_0^S}{n_0^N} = \left(\frac{T_0^N}{T_0^S}\right)^{1/2} \exp(\phi^S - \phi^N) \frac{1 - (1-a)\exp\left[-\dfrac{a\phi^N}{1-a}\right]}{1 - (1-a)\exp\left[-\dfrac{a\phi^S}{1-a}\right]}. \tag{11}$$

However, even in this static asymmetric model the electric field, $E_{\parallel}$, must depart from that of Equation (3), as a consequence of the additional electrostatic polarization induced into the plasma by the thermal effects resulting from the non-zero temperature gradient along the field line.

The existence of stationary Birkeland currents flowing in the exosphere, implies a high electric conductivity in the lower layers of the ionosphere. If this conductivity is not large enough to close the current loop, the electric potential difference ($\phi^N - \phi^S$) between the two conjugated exobase levels will eventually grow and reach the appropriate value to make the field aligned current, $j_{\parallel}$, equal to zero. Although in such an asymmetric case there will be no net electric charge flow, equal interhemispheric H^+ and electron fluxes from one ionosphere to the other will exist. This collisionless model is in some respect analogous to the hydrodynamic (collision-dominated) model with interhemispheric coupling developed by Mayr *et al.* (1972).

5.3. Collisionless models with rotation

The models of Eviatar *et al.* (1964) and Hartle (1969) do not include the rotation of the ionosphere-magnetosphere system. Although the centrifugal force remains small compared to the gravitational force for radial distances smaller than 5–6 Earth's radii,

the rotational effects play a significant role in the high altitude regions along the field lines $L>5$.

If $\Omega(r)$ is the angular velocity of a hydrogen plasma with respect to an inertial coordinate system, the reduced total potential energy of the particles along a given dipole magnetic field line L, is given by

$$q(\lambda; L) = \frac{m_{H^+} + m_e}{2} \frac{GM}{LR_E kT_0} \times \times \left[\frac{1}{\cos^2 \lambda_0} - \frac{1}{\cos^2 \lambda} + \frac{1}{3} \left(\frac{L}{L_c} \right)^3 (\cos^6 \lambda_0 - \cos^6 \lambda) \right], \tag{12}$$

where L_c is a critical parameter defined by

$$L_c = \left(\frac{2GM}{3\Omega^2 R_E^3} \right)^{1/3} \tag{13}$$

and where it is assumed that the rotational axis and magnetic dipole axis coincide (see Angerami and Thomas, 1964; Melrose, 1967). When the plasma corotates with the Earth, $\Omega(r)=\Omega_E=7.29\times10^{-5}$ rad s^{-1}, and $L_c=5.78$.

Along field lines with $L<L_c$, the potential given by Equation (12) has a maximum at the equator: $q(0; L)=q_{eq}$. In this case the density distribution in the rotating collisionless model can be obtained from formula (7) where q is now defined by (12).

Along field lines with $L>L_c$, the potential is a doubly peaked function of latitude and has two equal maxima, q_m, at latitudes $\pm\lambda_m$, with $\lambda_m=\arccos(L_c/L)^{3/8}$. In this case, the density distribution for a rotating collisionless model was obtained by Lemaire (1974):

$$\begin{aligned} n(\lambda; L) = n_0 \exp(-q) \Bigg\{ & \operatorname{erfc}[(q_m - q)^{1/2}] + \\ & + 2 \left(\frac{q_m - q}{\pi} \right)^{1/2} \exp(q - q_m) - (1-\eta)^{1/2} \exp\left(- \frac{\eta q}{1-\eta} \right) \times \\ & \times \left[\operatorname{erfc}(X^{1/2}) + 2 \left(\frac{X}{\pi} \right)^{1/2} \exp(-X) \right] + \\ & + \left(1 - \frac{\eta}{\eta_m} \right)^{1/2} \exp\left[\frac{\eta (q_m - q)}{\eta_m - \eta} \right] \times \\ & \times \left[\operatorname{erfc}(Y^{1/2}) + 2 \left(\frac{Y}{\pi} \right)^{1/2} \exp(-Y) + \right. \\ & \left. - \operatorname{erfc}(Z^{1/2}) - 2 \left(\frac{Z}{\pi} \right)^{1/2} \exp(-Z) \right] \Bigg\}, \end{aligned} \tag{14}$$

where $\operatorname{erfc}(x)$ is the complementary error function, and

$$X = \frac{q_m}{1-\eta_m} - \frac{q}{1-\eta}$$

$$Y = \frac{\eta_m q_m}{1-\eta_m} + \eta_m \frac{q_m - q}{\eta_m - \eta}$$

$$Z = \eta_m \frac{q_m - q}{\eta_m - \eta}$$

$$\eta_m = \frac{B(\lambda_m; L)}{B(\lambda_0; L)}.$$

Curve 4 in Figure 6 shows the relative equatorial density distribution, for a corotating collisionless model. This result is obtained from Equations (14) and (12) for $L > L_c = 5.78$, and from Equations (7) and (12) for $L < 5.78$, where q is replaced by q_{eq} and η by $a = B(0; L)/B(\lambda_0; L)$. The exobase temperatures, $T_0 = 1500$ K, and densities n_0, of the electrons and H^+ ions are equal and independant of the latitude λ_0. It can be seen that at large radial distances this equatorial density decreases approximately as L^{-4} (the L^{-4} variation is illustrated by curve 6 in Figure 6).

Curve 3 in Figure 6 illustrates the result obtained by Eviatar *et al.* (1964) for a non-rotating model. It can be seen that the rotation of the ionosphere-magnetosphere reduces the density at large radial distances when trapped particles are missing. Curves 1 and 2 correspond to diffusive equilibrium models with corotation ($\Omega = \Omega_E$) and without corotation ($\Omega = 0$) respectively. In the case of diffusive equilibrium the density increases with the rotational angular velocity Ω. This is also true in the lower part of the ion-exosphere for the collisionless model.

In the models (1) and (4) it was assumed that the ionosphere-magnetosphere system rotates with the same angular velocity as the Earth ($\Omega = \Omega_E$). However, outside of the plasmasphere the convection electric field, $E_\perp$, induced into the magnetosphere by the solar wind flow, changes significantly the azimuthal angular velocity $\Omega(\mathbf{r})$. Using the electric potential distribution E3 deduced by McIlwain (1972) from energetic particle flux measurements on board of the geosynchronous satellite ATS 5, it is possible to deduce the $\mathbf{E} \times \mathbf{B}$ drift velocity of the thermal plasma in the magnetosphere. From the E3 electric field distribution it is found that corotation is a very satisfactory approximation inside the plasmasphere. But for $L > 5$–7 the angular velocity

$$\Omega(\mathbf{r}) = \frac{|(\mathbf{E}_\perp \times \mathbf{B}) \times \mathbf{r}|}{B^2 r^2} \tag{15}$$

is in general quite larger than Ω_E. For instance at $L = 9$ in the 0200 LMT meridian plane $\Omega = 5.4\ \Omega_E$.

The dotted line in Figure 6 gives the relative equatorial density distribution when $\Omega(\mathbf{r})$ is deduced from McIlwain's electric field model E3 in the 2300 LMT meridian plane. Since the exobase boundary conditions are the same as in the collisionless models (3) and (4), the two times smaller density obtained for $L > 8$ in the model (5), results from the larger angular convection velocity in this magnetospheric region.

It can be concluded that the effect of rotation-convection plays a significant role on the thermal plasma distribution in the magnetosphere. Therefore this effect should not be neglected in future studies of the mid-latitude ionosphere-magnetosphere.

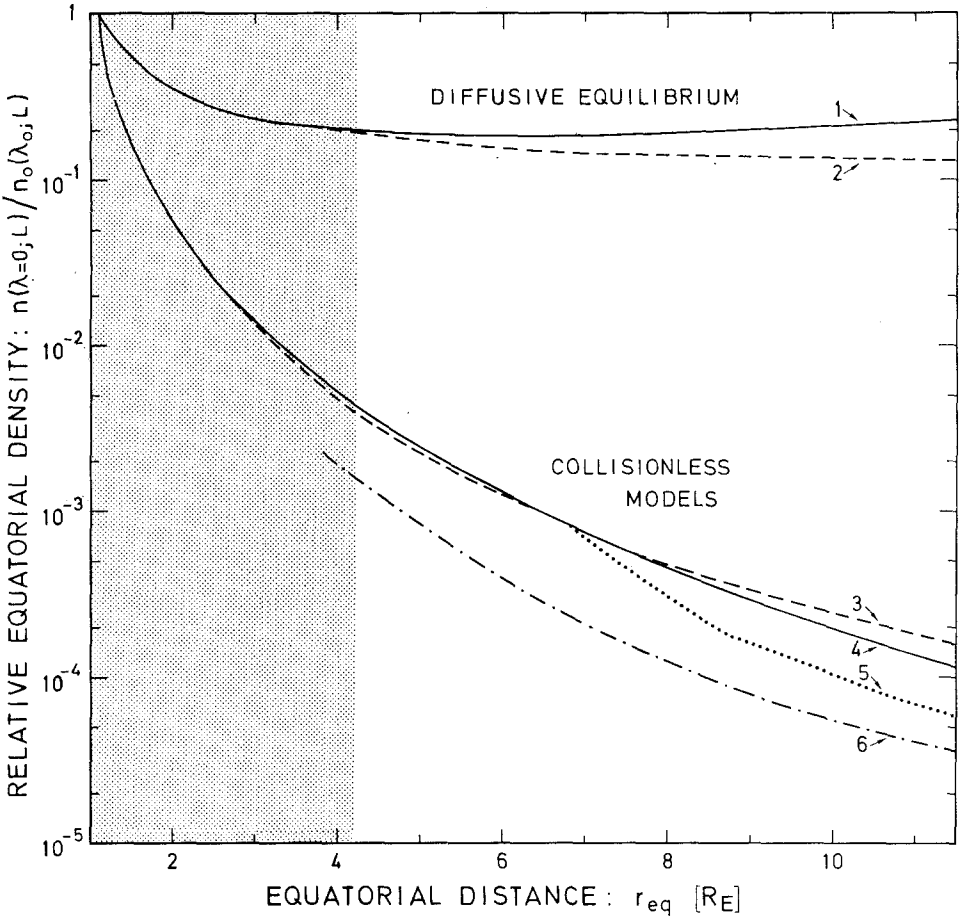

Fig. 6. *Relative equatorial densities in diffusive equilibrium and collisionless* (H^+, *e*) *ion-exosphere models.* The solid line (1) corresponds to a diffusive equilibrium model with a rotational speed, $\Omega = \Omega_E$, where Ω_E is the angular velocity of the Earth. The dashed line (2) corresponds to a non-rotating diffusive equilibrium model ($\Omega = 0$). The solid line (4) and the dashed line (3) correspond to collisionless models, respectively with, and without corotation. The dotted line (5) corresponds to a collisionless model with differential rotation where the angular velocity $\Omega(r)$ is calculated from the $\mathbf{E} \times \mathbf{B}$ drifts velocities deduced from McIlwain's (1972) E3 magnetospheric electric field distribution in the 2300 LMT meridian plane. In all these models the exobase temperature ($T_0 = 1500$K) and density $n_0(\lambda_0; L)$, were assumed to be independant of the latitude λ_0. The radial distance of the exobase is $r_0 = 1.1\ R_E$. The dot-dashed line (6) illustrates a L^{-4} density variation. The shaded area corresponds to the plasmasphere collision-dominated region.

Curves 3 and 7 in Figure 7 illustrate the relative equatorial density in symmetric collisionless models without rotation ($\Omega = 0$), when the exobase temperatures of the electrons and H^+ ions are increased from $T_0 = 1500$ K (curve 3) to $T_0 = 3000$ K (curve 7). Curves 4 and 8 correspond to symmetric collisionless models with corotation ($\Omega = \Omega_E$) for $T_0 = 1500$ K and $T_0 = 3000$ K, respectively. The larger exospheric densities (curves 7 and 8) result from the larger injection rate when the exobase temperature is higher. Indeed the increase of T_0 leads to an increase of the high-energy tail of the velocity

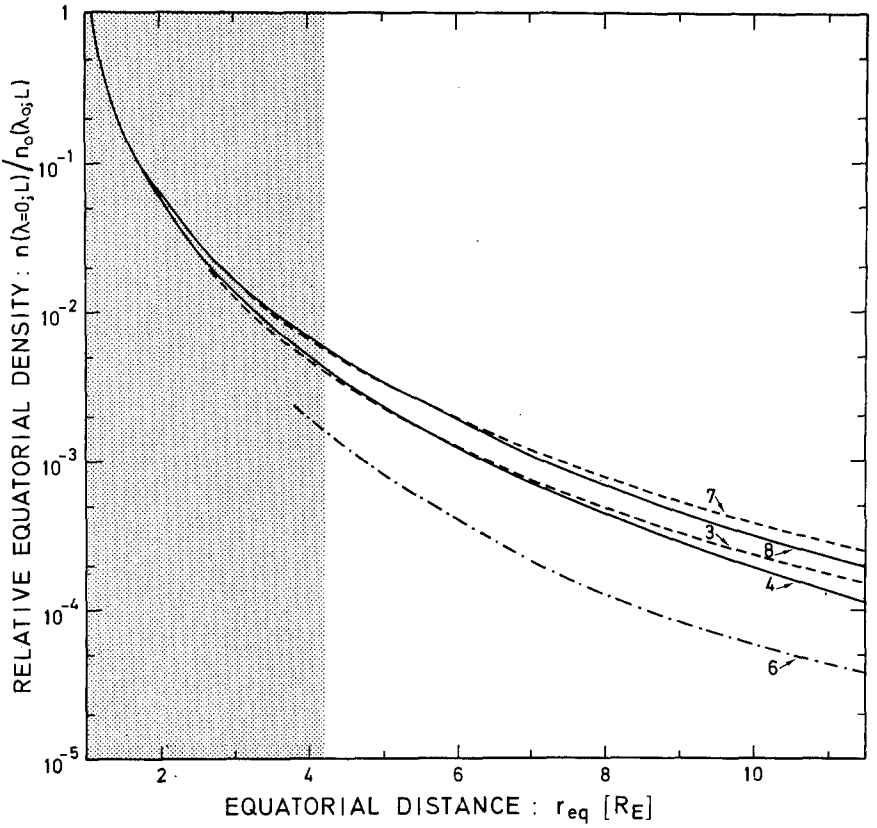

Fig. 7. *Effect of temperature on equatorial densities in collisionless symmetric* (H^+, *e*) *ion-exosphere models.* The solid line (4) and the dashed line (3) correspond to models with a uniform exobase temperature, $T_0 = 1500$K, respectively with, and without corotation. The solid line (8) and the dashed line (7) correspond to similar models for $T_0 = 3000$K. The L^{-4} density variation is shown by the dot-dashed line. The shaded area corresponds to the collision-dominated plasmasphere.

distribution of emergent particles with the consequence that more particles can reach higher altitudes.

5.4. Latitudinal Variation of the Exobase Conditions

In the preceding sections it was assumed that the exobase temperatures and densities are independent of the latitude and that H^+ was the only ionic constituant at the exobase level. Furthermore, the exobase was taken at a rather low altitude ($h_0 = 637$ km) as in Eviatar *et al.*'s (1964) and Hartle's (1969) numerical calculations. In Section 3 it was shown however that the exobase is located between 1000 km and 1500 km in the high- and mid-latitude regions, i.e. close to the OGO 6 orbit plotted in Figure 2. The ion mass spectrometer observations with this satellite have clearly demonstrated the strong latitudinal dependence of the H^+ and O^+ ion concentrations at an altitude of 1000 km. Beyond the light-ion-trough latitude, H^+ becomes a minor constituant and the contribution of the O^+ ions to the exobase density should be taken into account.

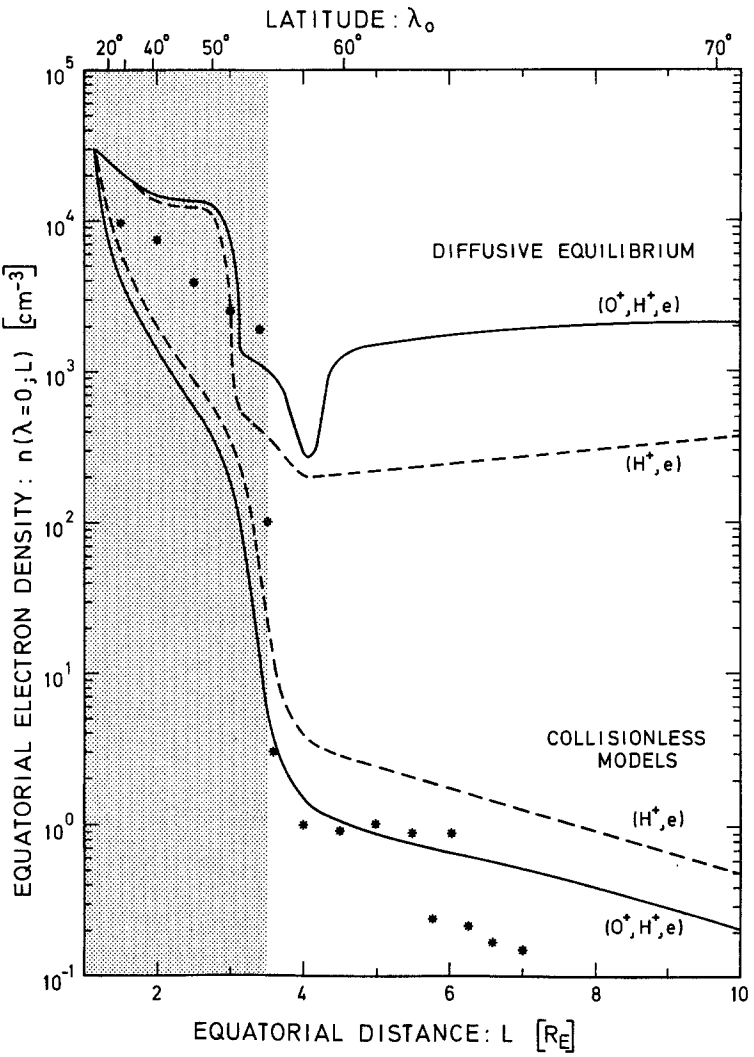

Fig. 8. *Effect of latitude dependent exobase conditions on the equatorial density distribution.* The solid lines correspond to a diffusive equilibrium and collisionless (O^+, H^+, *e*) ion-exosphere where the exobase ion densities are taken from Taylor's (1971a) measurements illustrated in Figure 2; the exobase levels correspond to the OGO 6 altitude. The exobase temperatures are also dependent on the latitude and are taken from Brace *et al.*'s (1967) electron temperature measurements at 1000 km. To illustrate the effect of heavy oxygen ions on the equatorial density distributions the dashed lines show similar model calculations when the O^+ ion concentration is taken zero. The asterisks correspond to near equatorial H^+ ion densities observed with OGO 5 by Chappell *et al.* (1970a) in the nightside region of the magnetosphere. The shaded area represents the plasmasphere.

In the model calculations presented in Figure 8 we assumed that the reference or exobase levels coincide with the altitude of the OGO 6 satellite. The H^+ and O^+ ion exobase densities are taken from Taylor's (1971a) ion mass spectrometer observations shown in Figure 2. The nearly symmetric latitudinal profiles illustrated in Figure 2

were obtained on September 23, 1969, at dawn, along the OGO 6 orbit, when the K_p index in the 12 h interval preceding the observations, was smaller than O^+. The exobase temperatures of the models in Figure 8 depend also on the latitude and are equal to the electron temperatures observed by Brace *et al.* (1967) in 1965 (at vernal equinox) with Explorer 32, orbiting at an altitude of 1000 km. The solid lines correspond to a three component exosphere (O^+, H^+, e) and the dashed lines to a two constituent model (H^+, e) without corotation. The two lower curves illustrate collisionless ion-exospheres whereas the two upper curves correspond to the case of diffusive equilibrium. Hence, the upper lines are only valid in the shaded area. Comparison between the dashed and solid lines shows the effect of O^+ ions at the 1000 km level on the ionization distribution. Despite their low concentration at high altitudes, these heavy ions strongly control the value of the H^+ and electron densities. The overall increase of the equatorial electron density for $L>4$, in the diffusive equilibrium (O^+, H^+, e) model results from the charge separation electric field $E_{\parallel}$ which, at low exospheric altitudes, is about 16 times larger than in the (H^+, e) model. Indeed, with a larger outward electric field the H^+ ions are pushed toward higher altitudes.

The asterisks in Figure 8 represent equatorial H^+ ion densities measured on March 25, 1968 with OGO 5 in the nightside region when the magnetic activity was rather high (K_p=4–5) (Chappell *et al.*, 1970a). The sharp decrease at $L=3.5$ corresponds to the plasmapause. Inside of the shaded plasmasphere area, the observed densities are significantly larger than the collisionless model predictions; this excess of density is due to the presence of a non negligible amount of trapped particles. Since the observed

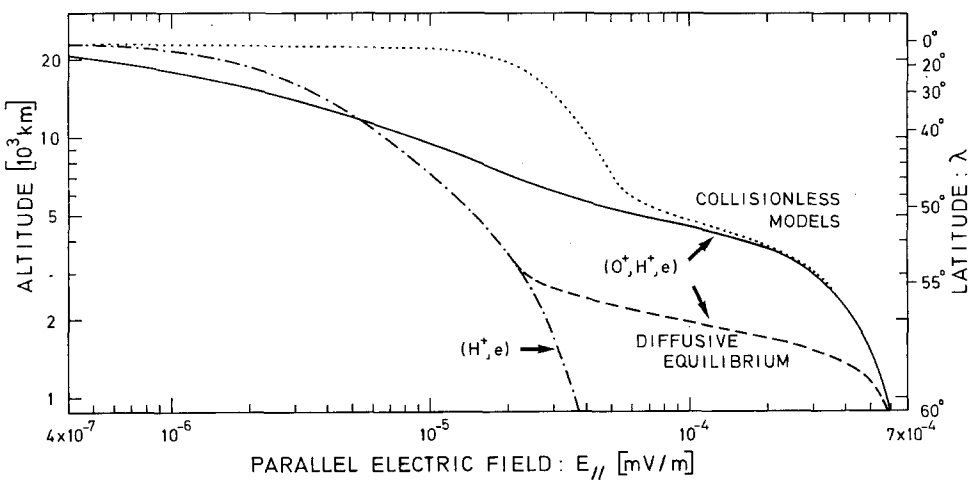

Fig. 9. *Parallel electric field distribution along the field line* $\lambda_0 = 60°\,N (L = 4.54)$. The dot-dashed line is the Pannekoek-Rosseland electric field distribution in a diffusive equilibrium and in a collisionless symmetric, non-rotating (H^+, e) exosphere, for $h_0 = 870$ km, $n_{H^+} = n_e = 5.8 \times 10^2$ cm^{-3}, $T_{H^+} = T_e = 2500$ K. The dashed line corresponds to the non-rotating symmetric diffusive equilibrium (O^+, H^+, e) exosphere for $h_0 = 870$ km, $n_{H^+} = 5.8 \times 10^2$ cm^{-3}, $n_{O^+} = 2 \times 10^4$ cm^{-3}, $T_{H^+} = T_{O^+} = T_e = 2500$ K (from Taylor, 1971a; Brace *et al.*, 1967). The dotted and solid line correspond to collisionless (O^+, H^+, e) models with, and without trapped electrons, respectively.

densities remain however smaller than the diffusive equilibrium values it seems that the trapped orbits are not saturated; i.e. the trapped particles probably are not in thermal equilibrium with the ballistic particles emerging from the ionosphere. Beyond the plasmapause the collisionless (O^+, H^+, e) model calculations are in quite good agreement with the observed values. Both decrease approximately as L^{-4}. Including the rotational speed would diminish the calculated equatorial density in this region, and the agreement would be even more satisfactory.

5.5. O^+ AND H^+ ION DISTRIBUTIONS ALONG A MAGNETIC FIELD LINE

Figure 9 gives the electric field distributions for different (O^+, H^+, e) exosphere models, along the geomagnetic field line ($L=4.54$) intersecting the exobase, located at 870 km altitude, at 60° dip latitude. The boundary conditions at the exobase are: $n_{H^+}=5.8\times10^2$ cm^{-3}, $n_{O^+}=2\times10^4$ cm^{-3}, $n_e=2.058\times10^4$ cm^{-3} (Taylor, 1971a), $T_{H^+}=T_{O^+}=T_e=2500$ K (Brace *et al.*, 1967). The solid line corresponds to the collisionless model with no trapped particles above the exobase. The dotted line shows the electric field when the trapped electrons are in thermal equilibrium with those emerging from the barosphere. For such a semi-kinetic model where the electrons are distributed according to the barometric law and where only the ions are supposed to be collisionless, the charge separation electric field is larger than for a model where all the particles are supposed to be collisionless. The dashed line in Figure 9 corresponds to the Pannekoek-Rosseland electric field in a (O^+, H^+, e) exosphere in diffusive equilibrium. The parallel electric field is deduced from Equation (3) with

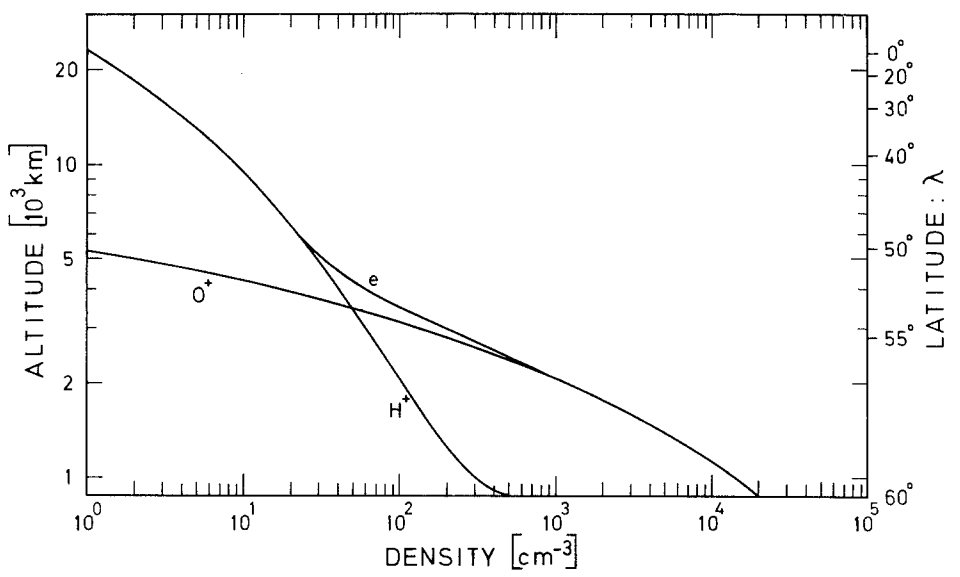

Fig. 10. *Ion and electron densities along the field line* $\lambda_0=60°$ ($L=4.54$) *in a non-rotating, symmetric collisionless model.* The exobase densities and temperatures are taken at $h_0=870$ km from Taylor (1971a) and Brace *et al.* (1967): $n_{H^+}=5.8\times10^2$ cm^{-3}, $n_{O^+}=2\times10^4$ cm^{-3}, $n_e=2.058\times10^4$ cm^{-3}, $T_{H^+}=T_{O^+}=T_e=2500$ K.

$m_+ = (n_{O^+} m_{O^+} + n_{H^+} m_{H^+})/(n_{O^+} + n_{H^+})$. To obtain the quasi-neutrality and to match ∇n_e to $\nabla(\Sigma_i n_i)$, a smaller electric field is required when the total ion density is enhanced by the presence of trapped ions. For comparison we also plotted the Pannekoek-Rosseland electric field in a two constituent (H^+, e) exosphere (dot-dashed line).

Figure 10 gives the electron, O^+ and H^+ ion densities in the previous discussed exospheric model without trapped particles. It can be seen that in this collisionless model the O^+ ions rapidly become a minor constituent above 3500 km along the mid-latitude closed field lines. Such a conclusion, which was already established in the case of diffusive equilibrium, remains valid when asymmetric boundary conditions or rotational effects are taken into account.

5.6. Plasmasheet particle precipitation

In the preceding sections we considered the distribution of the cold ionospheric plasma along closed magnetospheric field lines ignoring the high energy or suprathermal particles (50 eV–50 keV) observed in the magnetosphere. These hot electrons and protons are temporarily trapped in the distant geomagnetic field. It has been shown that the inner boundary of the plasmasheet in the equatorial plane, first observed by Gringauz *et al.* (1960a, b), is connected with the equatorward boundary of the auroral oval by means of the same magnetic field lines ($\Lambda \approx 70°$; $L \approx 10$) (Vasyliunas, 1970). The energy spectra of the plasmasheet electrons, which have generally a near maxwellian distribution, can be characterized by a temperature which is of the order of 10^7 K corresponding to an average energy of 1 keV (Bame *et al.*, 1967). The proton spectra have a similar shape, but their mean energy is usually several times larger: $T_{p^+} = 3\text{–}5 \times 10^7$ K (Bame, 1968). The observed plasmasheet electron and proton densities ($n_{ps.e}$ and n_{p^+}) are nearly equal, and range between 0.1 cm^{-3} to 0.5 cm^{-3} (Vasyliunas, 1970). The pitch angle distributions of the electrons and the protons are frequently isotropic for both constituents (Bame *et al.*, 1967; Hones, 1968). This hot plasmasheet gas is in direct contact with the much colder ionospheric plasma all over the auroral zone. The similarity of the energy and angular distributions of the plasmasheet particles (Hones *et al.*, 1971; Schield and Frank, 1970; DeForest and McIlwain, 1971) and the energetic particles observed in the auroral zones (Burch, 1968; Chase, 1970; Frank and Ackerson, 1971; Heikkila, 1972) demonstrate their common origin.

Since the density of the hot plasmasheet gas is comparable and generally larger than the equatorial density of the thermal ionospheric plasma ($n_{th.e} < 0.2$ cm^{-3} for $L > 10$, see Figure 8), its contribution to the total ionization density should be taken into account, at least at high altitudes along the auroral field lines. Since both the ionospheric and plasmasheet particles are collisionless above 1000 km altitude, the interpenetration problem of these two different plasmas must be studied by a kinetic theory and not by a classical hydrodynamic formulation. Therefore, unless we get evidence from future observations that wave-particle interactions are efficient enough to replace the Coulomb collisions in scattering and thermalising a significant fraction of the particles, a hydrodynamic treatment like that proposed by Hultqvist (1971, 1972) is not justified.

Kinetic descriptions of the interpenetration of the plasmasheet and the ionospheric particles have been given independently by Lemaire and Scherer (1973) and by Knight (1973). In Knight's model only the cold electrons evaporate from the ionosphere and the hot electrons emitted out of the plasmasheet at the equatorial plane, are supposed to carry the field aligned electric current. The electric potential difference between the baropause and the equatorial plane is calculated in order to obtain a given intensity of the electric current for a series of widely varying boundary conditions. In Knight's model the ion density distributions and the electric current carried by these particles are however not considered. In Lemaire and Scherer's kinetic model the contributions of the ionospheric O^+ and H^+ and of the plasmasheet protons is taken into account. Figure 11 shows the density distributions of the different types of ions and electrons along the auroral line $\lambda_0 = 71°$ ($L = 10.4$), when the velocity distributions of all particles are supposed to be Maxwellian and characterized by the following boundary conditions: (i) in the equatorial plane for the plasmasheet electrons and protons (Vasyliunas, 1970): $T_{ps.e} = 10^7$ K, $T_{p^+} = 5 \times 10^7$ K, $n_{ps.e} = 0.1$ cm^{-3}, $n_{p^+} = 0.1$ cm^{-3}; (ii) for the ionospheric electrons and ions at the 1000 km baropause altitude: $T_{th.e} = 4500$ K, $T_{O^+} = 1500$ K, $T_{H^+} = 4000$ K, $n_{O^+} = 2 \times 10^3$ cm^{-3}, $n_{H^+} = 2 \times 10^2$ cm^{-3}, $n_{th.e} = 2.2 \times$ $\times 10^3$ cm^{-3}. The ionospheric ion densities are quoted from Taylor *et al.*'s (1968) observations at the OGO 2 orbit above the northern auroral zone. These data were obtained in the duskside on October 1965 when the magnetic activity was low ($K_p < 1$).

The H^+ ion distribution in Figure 11 corresponds to the density of all the protons

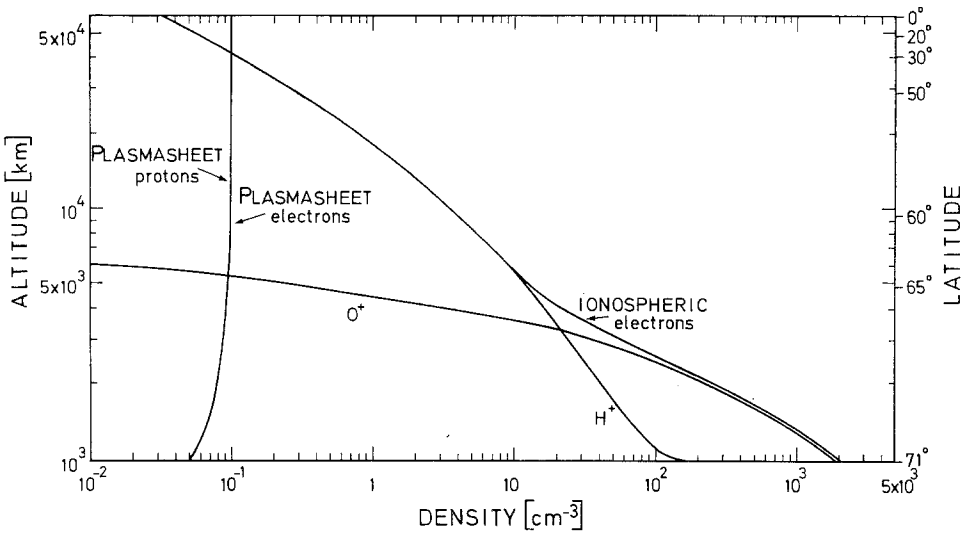

Fig. 11. *Ion and electron densities along an auroral field line in a collisionless model with plasmasheet particle precipitation.* The exobase temperatures and densities are given at $\lambda_0 = 71°$ and $h_0 = 1000$ km for the ionospheric ions and electrons by: $T_{\mathrm{th},e} = 4500$ K, $T_{O^+} = 1500$ K, $T_{H^+} = 4000$ K, $n_{O^+} = 2 \times 10^3$ cm^{-3}, $n_{H^+} = 2 \times 10^2$ cm^{-3}, $n_{\mathrm{th},e} = 2.2 \times 10^3$ cm^{-3}. The plasmasheet electron and proton temperatures and densities are given in the equatorial plane ($\lambda = 0$) at $h = 9.4\ R_E$ by: $T_{ps,e} = 10^7$ K, $T_{p^+} = 5 \times 10^7$ K, $n_{ps,e} = 0.1$ cm^{-3}, $n_{p^+} = 0.1$ cm^{-3}. For the plasmasheet particles there are no particles with pitch angles in the upward loss cone. For the ionospheric particles the pitch angle distribution is empty in the downward loss cone.

emitted at the top of the ionosphere in the northern hemisphere. Trapped orbits are not populated and the contribution of the ions emitted from the conjugated ionosphere are not taken into account in the present collisionless model. As a consequence an upward H^+ flux will result as in Hartle's (1969) asymmetric model. Such fluxes have actually been observed in the mid-latitude trough regions by Brinton *et al.* (1971). The thermal electrons and oxygen ions are also determined under the assumption that no particles emerging from the southern auroral ionosphere can reach the northern baropause. This assumption is justified by the fact that the transit time of the thermal ions from one hemisphere to the other, along field lines with $L > 10$, is comparable to the characteristic loss time for charge exchange or to the time it takes for a magnetic flux tube to be convected from the nightside to the dayside magnetopause, were its plasma content escapes into the tail along open field lines (Nishida, 1966). The plasmasheet electron and proton pitch angle distributions are supposed to be truncated in order to neglect the particles in the upward loss cone. This means that the precipitated plasmasheet particles (continuously injected or scattered into the downward loss cone) mirroring below the baropause are not reflected, but are scattered and lost by inelastic collisions into the denser part of the atmosphere.

The ionospheric O^+ and H^+ ion densities, shown in Figure 11, have a similar altitude variation as those obtained in the symmetric model illustrated in Figure 10 where no suprathermal particles are present. Therefore the presence of plasmasheet particles does not drastically change the thermal ion distributions along magnetic field lines (Lemaire and Scherer, 1973b). It is worthwhile to note that the often quoted large potential drops (1–10 kV) and the associated large parallel electric fields would, on the contrary, change considerably these thermal ion density distributions. From Figure 11 it also can be seen that the plasmasheet electron and proton densities increase slowly with altitude. This enhancement is due to the increase of the relative abundance of the trapped plasmasheet particles which mirror at high altitudes and which do not contribute to the density at lower levels. For the boundary conditions adopted in the present model calculation, the hot plasma density at high altitudes becomes more important than the cold ionospheric plasma density. This result agrees with Vasyliuna's (1970) conclusion that the very low energy (thermal or ionospheric) electron density is smaller than the density of the plasmasheet electrons observed in the 0.05–50 keV energy range.

Figure 12 illustrates the bulk velocities of the upward flowing hydrogen ions (solid line) and of the precipitated plasmasheet electrons and protons (dotted lines). It can be seen that at high altitudes the outward flow of H^+ ions becomes supersonic like in the polar wind models discussed in Section 6. The O^+ ion bulk velocity, not shown in Figure 12, remains smaller than 1 cm s^{-1}. The downward bulk velocities of the plasmasheet electrons and protons increases with decreasing altitudes, as if these particles were individually accelerated downwards by some large parallel electric field like that proposed by Hultqvist (1971, 1972). Nevertheless this apparent simultaneous acceleration of both the electrons and protons is not the consequence of the small polarization parallel electric field ($E_{\parallel} < 10^{-3}$ mV m^{-1}) but results simply from the

convergent geometry of the magnetic flux tubes. Indeed, since the plasmasheet particle densities are nearly uniform with altitude (see Figure 11), it results from particle flux conservation that the bulk velocities $w_{ps.e}$ and w_{p^+} are approximately proportional to A^{-1}, where A is the cross section of the magnetic field tube. Since $A \sim r^3$, the bulk velocities of the plasmasheet electrons and protons increase as r^{-3} when the radial distance decreases. The downward proton mean velocity is equal to 510 km s^{-1} at the exobase. This value is in quite good agreement with the observed values (300–500 km s^{-1}) deduced from Doppler shifts in Hα emissions in some auroral displays (Chamberlain, 1961).

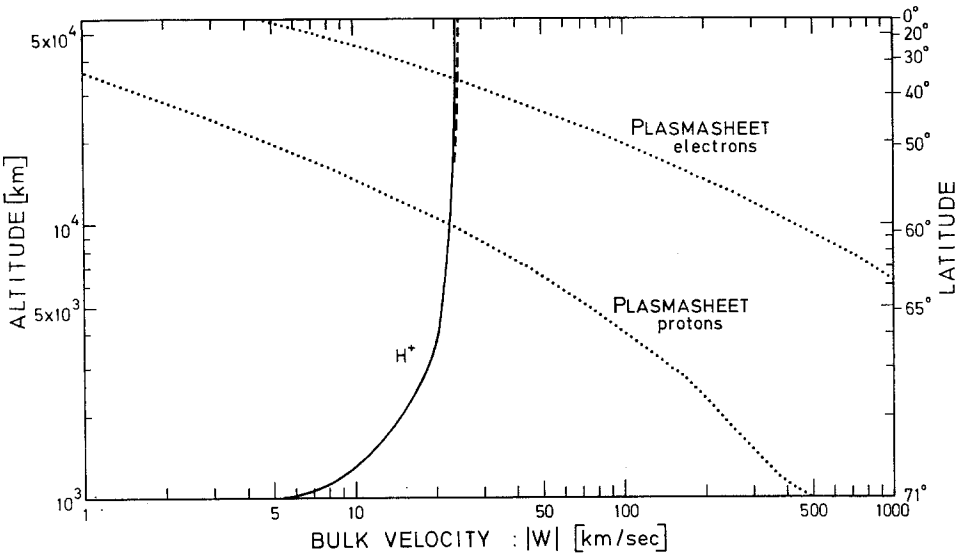

Fig. 12. *Bulk velocities of ionospheric and plasmasheet particles along an auroral field line.* The solid line corresponds to the upward mean velocity of the ionospheric H^+ ions emerging from the auroral ionosphere. The dotted lines correspond to the downward bulk velocities of the plasmasheet protons and electrons. The boundary conditions for this model calculation are the same as in Figure 11.

For the model illustrated in Figures 11 and 12, the particle fluxes across the reference level of 1000 km, are respectively $F_{H^+} = 9.2 \times 10^7$ cm^{-2} s^{-1}, $F_{O^+} = 6.6 \times 10^{-10}$ cm^{-2} s^{-1}, $F_{ps.e} = -4.9 \times 10^7$ cm^{-2} s^{-1}, $F_{p^+} = -2.5 \times 10^6$ cm^{-2} s^{-1}. The electric potential difference between the baropause and the equatorial plane is calculated in order to have a zero electric current; i.e. $F_{th.e} = F_{H^+} + F_{O^+} + F_{p^+} - F_{ps.e} = 1.387 \times 10^8$ cm^{-2} s^{-1}. This potential barrier $\Delta\psi_E$ is equal to -2.8 V in the present model. In the kinetic model proposed by Knight (1973) the electrons are assumed to carry the electric current

$$j_{\parallel} = -e(F_{ps.e} + F_{th.e}) \tag{15}$$

and the potential difference required to balance $F_{ps.e}$ by the escape flux $F_{th.e}$, is $\Delta\psi_E = -3.25$ V, for the same boundary conditions as in the model of Lemaire and Scherer (1973b). The difference between these two results must be attributed to the contribution of the H^+ ion flux which is neglected in the model of Knight.

5.7. Field Aligned Currents

The plasmasheet electron precipitation flux calculated in the preceding section is comparable to the lowest values observed by Frank and Ackerson (1971) and Heikkila (1972) at the low latitude boundary of the auroral region. However, much larger precipitation fluxes often are observed inside aurorae. Larger 1 keV electron downward fluxes are also required to explain the visible auroral displays (Chamberlain, 1961, p. 197, p. 253).

Models with larger precipitation fluxes can be obtained by increasing the plasmasheet electron density or temperature. Any increase of this precipitation flux will require a larger compensating escape flux of ionospheric electrons in order to maintain the field aligned current equal to zero. A smaller electric potential barrier, $\Delta\psi_E$, will then be required to obtain an enhanced upward flux of thermal electrons. However, there is a maximum or critical value beyond which $F_{th.e}$ cannot be increased:

$$F_c = \tfrac{1}{2} n_{th.e} \left(\frac{8kT_{th.e}}{\pi m_e} \right)^{1/2} \tag{16}$$

corresponding to the escape flux of thermal electrons when $\Delta\psi_E = 0$. For $n_{th.e} = 2.2 \times \times 10^3$ cm^{-3} and $T_{th.e} = 4500$ K, this limit is $F_c = 4.6 \times 10^{11}$ cm^{-2} s^{-1}. Beyond this value which corresponds approximately to the critical electric current deduced by Block (1972), a stable double potential layer can appear along the field line. Kindel and Kennel (1971) argued that ion cyclotron waves become unstable for precipitation fluxes larger than 10^9–10^{10} cm^{-2} s^{-1}. In these extreme cases strong wave particle interactions will change the physical properties of the plasma, and the present collisionless model will no more be applicable. The electric conductivity along the magnetic field direction will then be significantly reduced as a consequence of the triggered plasma turbulence. Larger potential differences arise between both ends of the field lines and large parallel electric fields can be observed on such occasions.

For plasmasheet precipitation fluxes much smaller than these thresholds, the potential difference necessary to satisfy the zero-electric-current condition, and the polarization electric field necessary to achieve the local quasi-neutrality, do not change significantly when $|F_{ps.e}|$ is increased from zero to the total ion flux:

$$F_i \approx F_{H^+} = \tfrac{1}{2} n_{H^+} \left(\frac{8kT_{H^+}}{\pi m_{H^+}} \right)^{1/2} \approx 10^8 \text{ cm}^{-2} \text{ s}^{-1}. \tag{17}$$

Nevertheless when the precipitated plasmasheet electron flux exceeds F_i the electric current transported by the plasmasheet electrons will remain partially unbalanced by the current transported by the upward flowing electrons of the ionosphere (Lemaire and Scherer, 1973b). Increasing the plasmasheet electron precipitation flux by $\Delta F_{ps.e}$ without changing the potential difference $\Delta\psi_E = -2.8$ V, nor the electric field, would result in an unbalanced upward field aligned current $j_\parallel = -e\Delta F_{ps.e}$, which can reach an intensity comparable to observed values, e.g. for $\Delta F_{ps.e} = -3.1 \times 10^9$ cm^{-2} s^{-1} the electric current density becomes 5×10^{-6} Am^{-2}.

If, on the contrary $F_{ps,e}$ is reduced to zero and $\Delta\psi_E$ remains unchanged, an electric current of -7.8×10^{-8} Am^{-2} will flow down into the ionosphere due to an excess of thermal electron flux escaping from the ionosphere. The intensity of this downward current can be increased tremendously by reducing slightly the potential barrier the thermal electrons have to overcome to escape across the equatorial plane into the conjugated hemisphere. Indeed in a collisionless model as illustrated in Figure 11, only a relatively small variation of $\Delta\psi_E$ from —2.8 V to —0.65 V would increase the thermal electron flux by two orders of magnitude and the field aligned current density would become -2.2×10^{-5} Am^{-2}. Birkeland currents observed in the auroral region sometimes have a density of the order of 5×10^{-6} Am^{-2} (Zmuda *et al.*, 1970; Choy *et al.*, 1971; Vondrak *et al.*, 1971; Aubry *et al.*, 1972) and can therefore be explained by a small variation of the potential difference $\Delta\psi_E$ or/and by an enhancement of the plasmasheet precipitation flux.

6. Collisionless Models for Open Magnetic Field Lines

In this section the application of the kinetic approach to the polar regions of the terrestrial ion-exosphere is described. We will not compare the results obtained by kinetic model calculations to the hydrodynamic (Banks and Holzer, 1968, 1969a, b, c; Marubashi, 1970a) and semi-kinetic (Holzer *et al.*, 1971) treatments of the polar wind since the domains of validity of each of these formulations have been reviewed elsewhere (Lemaire and Scherer, 1973a).

6.1. Exobase conditions

To determine the exobase level the electron density scale height and the ion mean free path can be deduced from observed density distributions in the topside polar ionosphere. Since the observational data usually belong to the collision dominated region of the ionosphere ($l<H_e$), the density distribution near the baropause can be obtained by upward integration of the hydrodynamic equations from the low altitude reference level where observational data are available. Among the infinite number of solutions depending on the initial value of the flow speed, the solution for which the diffusion flux equals the escape flux at the exobase must be chosen to match the hydrodynamic model of the collision dominated barosphere to the kinetic model of the collisionfree exosphere (Lemaire, 1972). The hydrodynamic solution selected in this way is in general different from Banks and Holzer's (1968) critical solution which gives a negligible small pressure at large radial distances when it is extended to the exospheric region. In the lower altitude range both solutions do not differ very much.

Quite accurate values for the ion densities in the polar regions have been obtained from the OGO 2 mass spectrometer measurements (Taylor *et al.*, 1968). For the dusk region of the summer polar cap at a dipole latitude of 85°S and at an altitude of 950 km values for the ion concentrations are given by

$$n_{O^+} = 7\times10^3 \text{ cm}^{-3}, \qquad n_{H^+} = 3.2\times10^2 \text{ cm}^{-3}, \qquad n_{He^+} = 7 \text{ cm}^{-3}.$$

Moreover the electron and ion temperatures are assumed to be

$$T_e = 4500\,\mathrm{K}, \qquad T_{O^+} = 1500\,\mathrm{K}, \qquad T_{H^+} = 4000\,\mathrm{K}, \qquad T_{He^+} = 3750\,\mathrm{K}.$$

These unequal temperature values can be justified by the fact that heating by conduction and energy transport by convection will influence in a different way the electrons, the heavy ions and the lighter ions. Moreover, the density scale height deduced from OGO 2 and OGO 4 measurements (Taylor *et al.*, 1968; Taylor, 1971b) or from Alouette I experiments (Thomas and Rycroft, 1970) can be interpreted with these temperature values.

Starting with these densities and temperatures as boundary conditions the hydrodynamic continuity and momentum equations described by Banks and Holzer (1968, 1969b) can be integrated upwards. To take account of the production and interactions between ionized and neutral particles, the neutral atmosphere model of Nicolet and Kockarts (private communication, 1971) corresponding to an exosphere temperature $T_N = 1000\,\mathrm{K}$, was adopted. Due to the high temperature of the hydrogen ions the exobase is located at a rather low altitude $h_0 = 960$ km. At this level the calculated densities and upward diffusion fluxes are

$$n_e = 7154.68\ \mathrm{cm}^{-3}; \quad n_{O^+} = 6844.80\ \mathrm{cm}^{-3};$$
$$n_{H^+} = 303.23\ \mathrm{cm}^{-3}, \quad n_{He^+} = 6.65\ \mathrm{cm}^{-3}$$

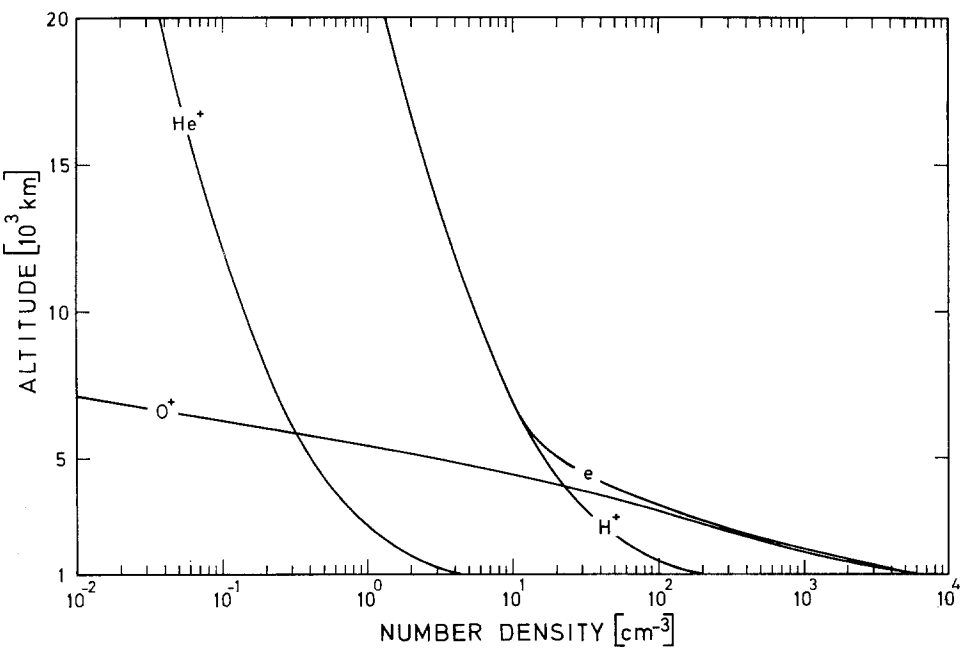

Fig. 13. *Electron and ion number densities along an open geomagnetic field line intersecting the exobase at* 85° *dip latitude.* The exobase is located at 960 km altitude and the trapped orbits are not populated. The exobase conditions are: $n_e = 7154.68\ \mathrm{cm}^{-3}$; $n_{O^+} = 6844.80\ \mathrm{cm}^{-3}$; $n_{H^+} = 303.23\ \mathrm{cm}^{-3}$; $n_{He^+} = 6.65\ \mathrm{cm}^{-3}$; $T_e = 4500\,\mathrm{K}$; $T_{O^+} = 1500\,\mathrm{K}$; $T_{H^+} = 4000\,\mathrm{K}$, $T_{He^+} = 3750\,\mathrm{K}$.

$$F_e = 1.38 \times 10^8 \text{ cm}^{-2} \text{ s}^{-1}, F_{O^+} = 0; F_{H^+} = 1.37 \times 10^8 \text{ cm}^{-2} \text{ s}^{-1};$$
$$F_{He^+} = 1.45 \times 10^6 \text{ cm}^{-2} \text{ s}^{-1}.$$

These values are used as boundary conditions in the kinetic model calculations for the polar ion-exosphere discussed in the ensuing sections.

6.2. Exospheric densities and the electric field

The electron and ion number densities are plotted in Figure 13 for a model in which the trapped orbits in the ion-exosphere are not populated. It can be seen that the oxygen ion density decreases much more rapidly with altitude than the H^+ and He^+ concentrations. Ionized oxygen which is the dominant ionic constituent at the baropause level becomes a minor constituent at 6000 km altitude. The O^+ concentration equals the H^+ and He^+ concentrations at 4000 km ($n_{H^+} = n_{O^+} = 23.5 \text{ cm}^{-3}$) and at 5900 km ($n_{He^+} = n_{O^+} = 0.3 \text{ cm}^{-3}$), respectively. Above 6000 km the hydrogen ion density is almost equal to the electron density, and the He^+ and H^+ density scale heights are practically the same. At 3000 km the calculated oxygen and hydrogen ion densities ($n_{O^+} = 128 \text{ cm}^{-3}$; $n_{H^+} = 35.8 \text{ cm}^{-3}$) are in quite good agreement with the experimental

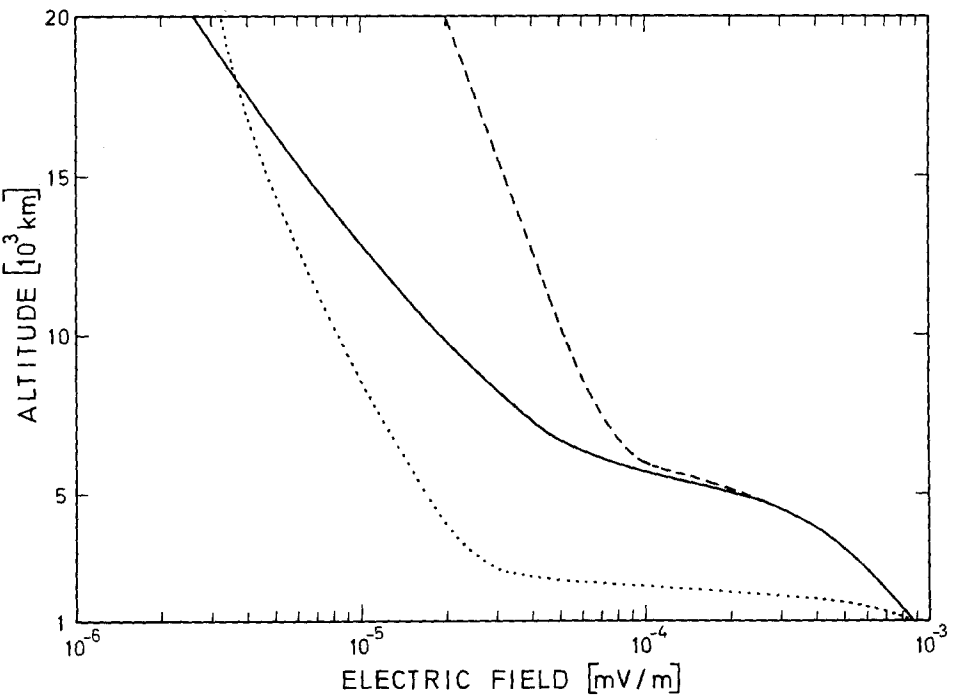

Fig. 14. *Electric field strength along an open geomagnetic field line intersecting the exobase at 85° dip latitude.* At the exobase, located at 960 km altitude, the boundary conditions are: $n_e = 7154.68 \text{ cm}^{-3}$; $n_{O^+} = 6844.80 \text{ cm}^{-3}$; $n_{H^+} = 303.23 \text{ cm}^{-3}$; $n_{He^+} = 6.65 \text{ cm}^{-3}$; $T_e = 4500 \text{ K}$; $T_{O^+} = 1500 \text{ K}$; $T_{H^+} = 4000 \text{ K}$; $T_{He^+} = 3750 \text{ K}$. The solid line corresponds to the model in which the trapped orbits are not populated, the dashed and dotted lines correspond respectively to the 'trapped' model and to the case of diffusive equilibrium.

results ($n_{O^+} = 80$–$200\ cm^{-3}$; $n_{H^+} = 30$–$50\ cm^{-3}$) obtained by Hoffman (1970, 1971) with the Explorer 31.

In the case of diffusive equilibrium, ionized hydrogen would become the most abundant constituent at a much lower altitude (1500 km) and the oxygen ion density would become less important than the He^+ density in the region above 2300 km. The oxygen ion density scale height is slightly smaller in the diffusive equilibrium model than in the polar wind as a consequence of the smaller parallel electric field near the exobase (see Figure 14). The upward directed charge separation electric fields, shown in Figure 14 by the solid line for the collisionless model and by the dotted line for the case of diffusive equilibrium, counters the gravitational pull on the ions and adapts the electron density scale height to the total ion density scale height. The intensity of the electric field is such that the total ion flux equals the electron flux and that the quasi-neutrality condition is satisfied. Figure 14 clearly shows that the electric force acting on the charged particles is larger when the ions are allowed to escape than for the case of diffusive equilibrium. This is true at least in the lower part of the exosphere. At higher altitudes where the H^+ and He^+ flow speeds are already supersonic (see Figure 15) the electric field decreases more rapidly in the polar wind model than in the static model. Above 18000 km the polar wind electric field intensity is the smaller one.

The assumption that the trapped orbits for the electrons and oxygen ions are completely filled, and that the trapped particles are in statistical equilibrium with the particles coming from the barosphere, does not change significantly the total number densities of the electrons, and the hydrogen and helium ions. In such a 'trapped' model the O^+ concentration, however, is affected much more, especially at large distances from the exobase. This is because at high altitudes the ballistic components becomes less important than the trapped component; the escaping component for O^+ being negligible small (see also Lemaire and Scherer, 1971).

Adding trapped particles changes the electric field significantly as can be seen from Figure 14 where the dashed line corresponds to the 'trapped' model. If trapped electrons are taken into account, the electric field will increase. When trapped electrons contribute to the total electron density, a larger electric field is required to reduce the electron density to the hydrogen ion density. Finally it is worthwhile to note that everywhere in the exosphere the electric field in a 'trapped' model remains larger than in a diffusive equilibrium model; at large radial distances the rate of decrease is in both cases practically equal.

6.3. Bulk velocities or flow speeds

The escape fluxes of the charged particles in the polar ion-exosphere are determined by the potential energy differences between the exobase and infinity. The reduced total potential energies (in kT units) are plotted for each species in Figure 15. It can be seen that the electrons and the oxygen ions coming from the barosphere meet a potential barrier, and consequently they are decelerated by the combined effect of the gravitational and electric field. The hydrogen and helium ions, on the contrary, will be accelerated outwards since their potential energy is smaller in the exosphere than at the

baropause. Note that for the model under consideration, the helium ions have a minimum potential energy at 5500 km; i.e. at the altitude where the electric field distribution in the exosphere has an inflection point. Below this level the H^+ and He^+ are accelerated to supersonic flow speeds as illustrated in Figure 16. Above 5500 km the electric field decreases less rapidly and the helium ions are slightly decelerated. Since the minimum of the H^+ potential energy is located at infinity these particles will be accelerated in the whole exosphere. At large radial distances the H^+ and electron flow speeds tend asymptotically to a constant value (≈ 24 km s^{-1}).

The O^+ flow speed which is also plotted in Figure 16 (upper logarithmic scale) is extremely small and negligible compared to the bulk velocities of the other constituents. This is because the gravitational pull acting on the heavy oxygen ions is much more important than the outward directed electric force, and consequently the oxygen ions are tied to the earth. Only a few oxygen ions with very large thermal velocities can escape into the geomagnetic tail. In a 'trapped' model (i.e. O^+ and electron trapped orbits filled) the bulk velocities of the hydrogen and helium ions are slightly

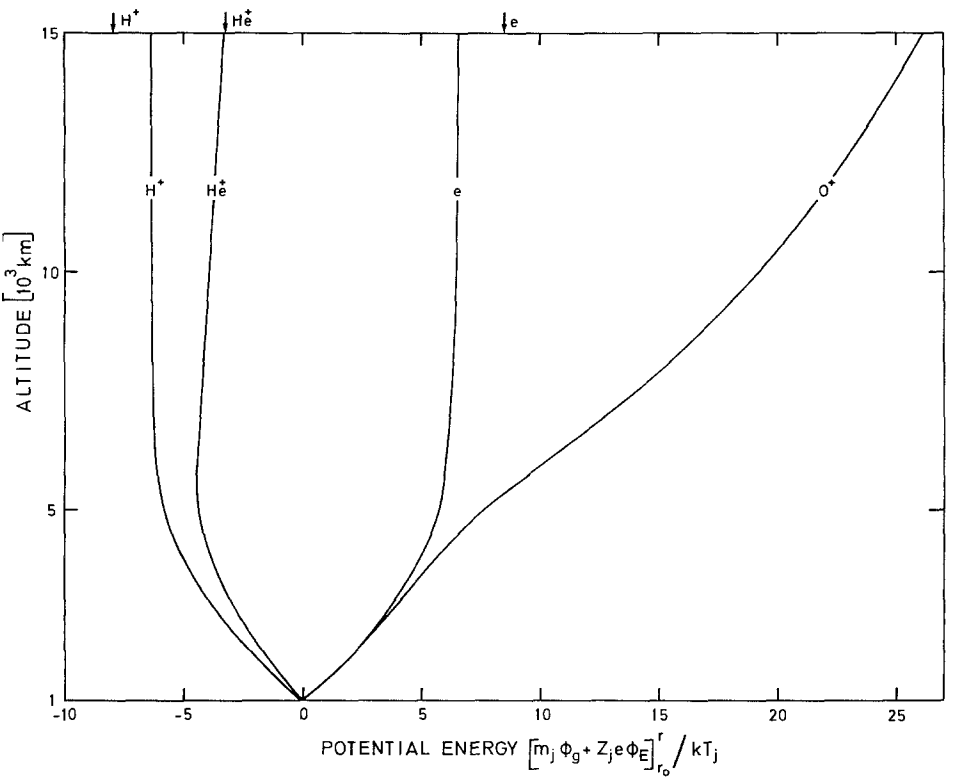

Fig. 15. *Reduced potential energies along a geomagnetic field line intersecting the exobase at* 85° *dip latitude.* The trapped orbits are not populated and at the exobase level, situated at 960 km altitude, the boundary conditions are: $n_e = 7154.68$ cm^{-3}; $n_{O+} = 6844.80$ cm^{-3}; $n_{H+} = 303.23$ cm^{-3}; $n_{He+} = 6.65$ cm^{-3}; $T_e = 4500$K; $T_{O+} = 1500$K; $T_{H+} = 4000$K; $T_{He+} = 3750$K. The asymptotic values are indicated by arrows; for the oxygen ions this asymptotic value is 40.

larger because of the larger electric field. Nevertheless the most salient properties discussed above remain unchanged.

Finally it is worthwhile to note that at 3000 km altitude the calculated escape fluxes (=densities × bulk velocities) for the hydrogen and helium ions are $F_{H^+} = 6.6 \times 10^7$ cm^{-2} s^{-1} and $F_{He^+} = 7.0 \times 10^5$ cm^{-2} s^{-1}, whereas observations made by Hoffman (1968, 1970, 1971) yielded $F_{H^+} = 5 \times 10^7$ cm^{-2} s^{-1} and $F_{He^+} = 5 \times 10^5$ cm^{-2} s^{-1}.

6.4. Influence of Photoelectrons

The polar wind concept was introduced by Axford (1968), who argued that a photoelectron efflux of 2×10^8 cm^{-2} s^{-1} is required at 400 km altitude to drag into the magnetotail the protons and helium ions produced in the sunlit ionosphere. Nagy and Banks (1970), and Shawhan *et al.* (1970) have shown that photoelectron fluxes of this order of magnitude escape from the sunlit ionosphere. Moreover, Maier and Rao (1970) and Heikkila (1971) recently observed in the high altitude ($\approx$2000 km) suprathermal (i.e. with an energy larger than 5 eV) electron fluxes of 5–10 $\times 10^7$ cm^{-2} s^{-1}.

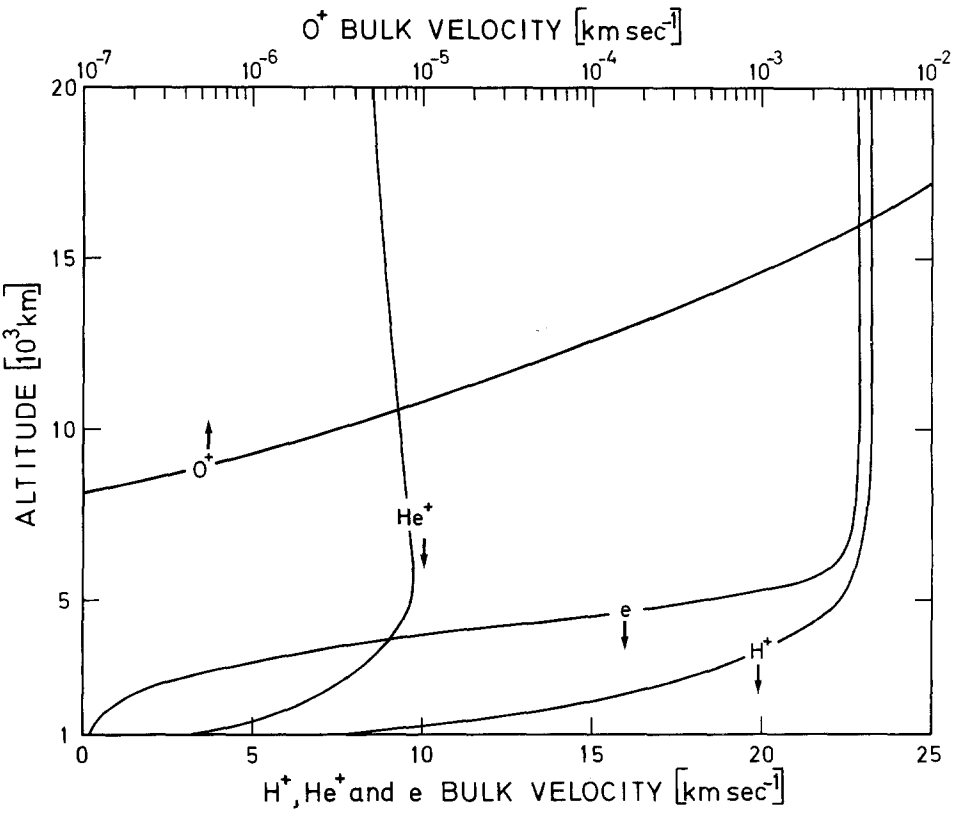

Fig. 16. Bulk velocities for the electrons, H^+ and He^+ (lower scale), and for O^+ (upper scale) in a polar wind model with exobase conditions: $n_e = 7154.68$ cm^{-3}; $n_{O^+} = 6844.80$ cm^{-3}; $n_{H^+} = 303.23$ cm^{-3}; $n_{He^+} = 6.65$ cm^{-3}; $T_e = 4500$ K; $T_{O^+} = 1500$ K; $T_{H^+} = 4000$ K; $T_{He^+} = 3750$ K. The exobase is located at 960 km altitude, and the trapped orbits are not populated.

In this section we will discuss how the ionospheric plasma flow in the polar regions will be modified by increasing values of the photoelectron flux.

Since the escape flux of the hydrogen and helium ions is completely determined by the baropause conditions ($n_{H^+}=303\ cm^{-3}$, $T_{H^+}=4500\,K$; $n_{He^+}=6.65\ cm^{-3}$, $T_{He^+}=$ $=3750\,K$) the total photoelectron flux ($F_{ph.e}$) cannot much exceed the H^+ efflux, unless the thermal electron gas implodes (i.e. $F_{th.e}<0$) or unless field aligned currents are allowed to flow into the ionosphere. Adding a photoelectron flux at the exobase will increase the potential barrier the escaping thermal electrons have to overcome, in order to adjust the total electron flux to the total positive ion flux which is mainly given by the H^+ efflux. Table I, coulumn (a) gives the potential energy barrier for the electrons in five polar wind models which only differ by the value of the photoelectron escape flux at the base of the ion-exosphere. As long as the photoelectron flux is small,

TABLE I

The effect of a photoelectron efflux at the exobase on the minimal escape energy for an electron (column (a)); columns (b), (c) and (d) give respectively the number density for the ballistic and escaping electrons, and the electron bulk velocity at 10000 km altitude, under the asumption that no trapped particles are present

Photoelectron efflux ($cm^{-2}\ s^{-1}$)	(a) (eV)	(b) (cm^{-3})	(c) (cm^{-3})	(d) ($km\ s^{-1}$)
0	3.3	5.31	0.21	22.8
5×10^7	3.5	5.39	0.13	14.7
10^8	3.8	5.46	5×10^{-2}	6.7
1.40×10^8	5.4	5.50	9×10^{-4}	0.17
1.41×10^8	6.8	5.50	2×10^{-5}	0.005

the increase of the potential barrier remains small too. This potential barrier however becomes much more important when the photoelectron flux almost equals the total hydrogen and helium ion flux ($F_{H^+}+F_{He^+}=1.41006\times10^8\ cm^{-2}\ s^{-1}$). As a consequence of the enlarged potential barrier, the number density of the escaping electrons will decrease (see Table I, column c), whereas the number density of the ballistic electrons (see Table I, column b) will increase, the total electron density remaining practically unchanged. Therefore the escape flux of the thermal electrons will diminish with the added photoelectron flux and the electron bulk velocity (see Table I, column d) will decrease too. The flow speed of the thermal electrons is plotted in Figure 17 for different models ($F_{ph.e}=0$; $5\times10^7\ cm^{-2}\ s^{-1}$; $10^8\ cm^{-2}\ s^{-1}$). The general pattern of the electron bulk velocity distributions is the same for the three models: the flow speed increases rapidly just above the exobase and tends asymptotically to a constant value at large radial distances. The asymptotic value of the electron flow speed, however depends very strongly on the value of the photoelectron efflux. The hydrogen ion bulk velocity which is also shown in Figure 17 does not change with the photoelectron flux. Since the total density distributions for each species are not altered significantly by adding a photoelectron efflux the charge separation electric field which provides the quasi-neutrality everywhere in the exospheric plasma, will remain unchanged too.

The preceding conclusions are only true for the case that the trapped orbits are empty. The electric field in a 'trapped' model will be greatly influenced by the presence of photoelectrons. Figure 18 illustrates the electric field distribution for three 'trapped' polar wind models which differ only by the photoelectron efflux at the exobase level, respectively given by $F_{ph.e}=0$; 10^8 cm^{-2} s^{-1}, and 1.4×10^8 cm^{-2} s^{-1}. It can be seen that the electric field increases significantly with an enhancement of the photoelectron

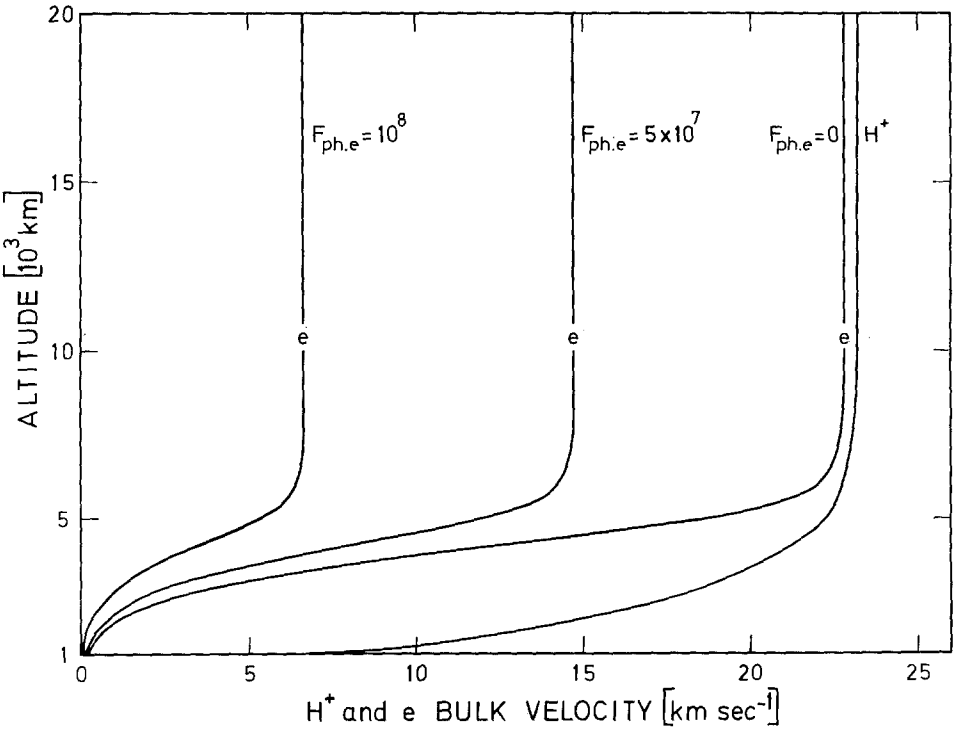

Fig. 17. Electron and H^+ bulk velocities in three polar wind models which differ by the value of the photoelectron flux $F_{ph.e}$ (cm^{-2} s^{-1}) at the exobase located at 960 km altitude. The trapped orbits are not populated, and the exobase conditions are: $n_e=7154.68$ cm^{-3}; $n_{O^+}=6844.80$ cm^{-3}; $n_{H^+}=303.23$ cm^{-3}; $n_{He^+}=6.65$ cm^{-3}; $T_e=4500$K; $T_{O^+}=1500$K; $T_{H^+}=4000$K; $T_{He^+}=3750$K.

TABLE II

The effect of a photoelectron efflux at the exobase, on the number density of the ballistic (column (a)), escaping (column (b)), and trapped (column (c)) electrons at 10000 km altitude; the total electron density and the electron bulk velocity at 10000 km are reported in column (d) and (e), respectively; column (f) gives the H^+ bulk velocity at 10000 km altutide

Photoelectron efflux (cm^{-2} s^{-1})	(a) (cm^{-3})	(b) (cm^{-3})	(c) (cm^{-3})	(d) (cm^{-3})	(e) (km s^{-1})	(f) (km s^{-1})
0	3.483	0.235	1.648	5.366	23.49	23.85
5×10^7	3.285	0.139	1.901	5.326	15.28	24.03
10^8	3.039	0.55×10^{-1}	2.183	5.278	6.95	24.25
1.40×10^8	2.783	0.9×10^{-3}	2.448	5.233	0.17	24.46
1.41×10^8	2.775	0.2×10^{-4}	2.455	5.231	0.005	24.46

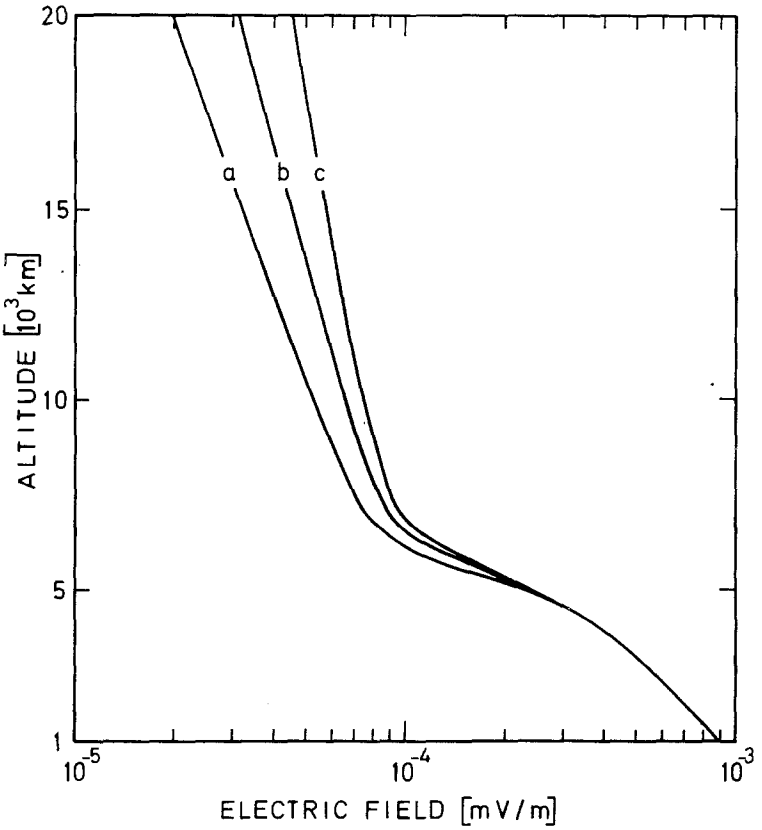

Fig. 18. *The electric field strength along a geomagnetic field line intersecting the exobase at* 85° *dip latitude.* The exobase is located at 960 km altitude, and the trapped orbits are completely filled with oxygen ions and electrons. The exobase conditions are: $n_e = 7154.68\ \mathrm{cm}^{-3}$; $n_{O+} = 6844.80\ \mathrm{cm}^{-3}$; $n_{H+} = 303.23\ \mathrm{cm}^{-3}$; $n_{He+} = 6.65\ \mathrm{cm}^{-3}$; $T_e = 4500\mathrm{K}$; $T_{O+} = 1500\mathrm{K}$; $T_{H+} = 4000\mathrm{K}$; $T_{He+} = 3750\mathrm{K}$. The models differ by the values of the photoelectron flux at the exobase: (a) $F_{ph,e} = 0$; (b) $F_{ph.e} = = 10^8\ \mathrm{cm}^{-2}\ \mathrm{s}^{-1}$; (c) $1.4 \times 10^8\ \mathrm{cm}^{-2}\ \mathrm{s}^{-1}$.

efflux; the differences between the electric fields becoming more important with altitude. This augmentation of the electric field is due to the presence of trapped electrons. Indeed, as a consequence of the enlarged potential barrier the number density of the trapped particles (see Table II, column c) will become more important since the most remote mirror points will be brought nearer to the exobase. Therefore, a stronger electric field is set up to maintain the quasi-neutrality. This enhanced electric field diminishes the number densities of the ballistic electrons (see Table II, column a); the decrease in the number density of the escaping particles (see Table II, column b) is mainly due to the higher potential barrier. The total electron density (see Table II, column d) consisting of ballistic, escaping and trapped particles does not change significantly by adding a photoelectron flux. The thermal electron flow speed will decrease very much in the presence of a photoelectron flux due to the higher potential barrier. The H^+ and He^+ bulk velocity on the contrary will become slightly larger as a consequence of the enhanced electric field intensity which accelerates the hydrogen

and helium ions outwards. This is illustrated in columns (e) and (f) of Table II, where the bulk velocities of the electrons and protons at 10000 km altitude are reported for different polar wind models.

7. Conclusions

Although the kinetic theory was used since its origin, to study the escape of neutral particles from a planetary atmosphere, it is only during the last two decades, that full attention has been given to the problem of charged particles in an ion-exosphere. After a period of controversies during which the classical hydrodynamic theory was preferred to the kinetic theory, it is now recognized that both approaches are not contradictory but are complementary, when the charge separation electric field in the collisionless plasma is correctly evaluated. The CGL approximation which is sometimes used when the thermal ions are collisionless and the electrons collision-dominated, is physically equivalent to the kinetic formulation, but has the disadvantage to become rather cumbersome when more than one ionic constituent must be taken into account or when suprathermal electrons or ions must be considered in the exospheric system.

The ionospheric plasma becomes collisionless above the ion-exobase surface coinciding with the plasmapause, and located near 1000 km altitude in the trough and polar regions; i.e. at a much larger altitude than the exobase for neutrals. Due to the existence of closed and 'open' field lines in the magnetosphere, collisionless models for subauroral regions must be distinguished from those of the polar regions where the ionospheric plasma can escape into the magnetotail.

As a consequence of the constraint for charged particles to move along non-radial magnetic field lines, the ion density in collisionless exosphere models with closed magnetic field lines, decreases with dipole latitude and reaches a minimum at the equator. Non-symmetric boundary conditions at the conjugate points where the field line intersects the ion-exobase show that interhemispheric particle fluxes exist from the denser or/and hotter hemisphere to the less dense or/and colder ionosphere. Therefore the charge separation electric field is no longer given by the Pannekoek-Rosseland field which remains valid for symmetric boundary conditions in a two-constituent ion-exosphere. An angular rotation of the ionosphere-magnetosphere system decreases the equatorial density distribution, and a temperature increase at the ion-exobase results in an enhancement of the ionization density along the whole magnetic field line.

When the exobase ion densities and temperatures vary with dipole latitude, the calculated equatorial density in collisionless models show a rapid decrease at a radial distance corresponding to the plasmapause or knee position. Beyond this height the collisionless equatorial density decreases approximately as L^{-4} which is in agreement with observations. Although the ionized oxygen becomes rapidly a minor constituent in the exosphere, its presence at the high latitude exobase level influences significantly the ionization density at large radial distances in the magnetosphere.

The kinetic description is particularly appropriated to study the interpenetration of the cold ionospheric plasma and the suprathermal plasma of magnetospheric origin. The study of plasmasheet particle precipitation shows that for normal plasmasheet

electron and proton densities and temperatures, the charge separation electric field and the ionospheric ion distributions are not much changed by adding these suprathermal particles in the system. However, if the energetic electron density or mean energy is suddenly enhanced, the precipitation flux can become so large that it is no more balanced by the upward flux of the cold electrons. Field aligned currents are then expected to flow between the auroral ionosphere and the plasmasheet. Moreover if the plasmasheet precipitation flux exceeds a critical intensity, ion-cyclotron and ion-accoustic waves will become unstable and trigger plasma turbulence, decreasing the electric conductivity along the field line. For extremely large precipitation fluxes stable double potential layers can eventually occur. Under normal conditions however the potential difference between the ionosphere and the plasmasheet is approximately-3 V, at least when the density of the field aligned currents flowing up or down along the auroral field lines, is smaller than 10^{-5} A m^{-2}.

For the case of open magnetic field lines, the exospheric densities of ionized oxygen, hydrogen, and helium in the collisionless polar wind model are quite different from that of diffusive equilibrium. The electric field distribution in kinetic models with or without trapped electrons, is also quite different from that of the Pannekoek-Rosseland field which is valid in the case of diffusive equilibrium. The bulk velocities of the light hydrogen and helium ions become rapidly supersonic in the exosphere as a consequence of the upward electric force. The flow speed of the oxygen ions remains, however, extremely small in the polar wind. The addition of escaping photoelectrons to the system does not change much the ion density distributions but it decreases mainly the thermal electron efflux and bulk velocity. The largest effect is obtained on the electric field distribution when trapped electrons are supposed to be present in the kinetic model.

Comparison of collisionless model calculations with observations at high altitudes in the ion-exosphere or in the magnetosphere show generally a satisfactory agreement. This leads to the conclusion that the kinetic theory is not only an academic concept but a very useful tool of investigation in space physics.

Appendix A. Classification of the Exospheric Particles

In a diffusive equilibrium isothermal ionosphere with closed magnetic field lines the charge separation electric field is given by the Pannekoek-Rosseland field

$$\mathbf{E}(\mathbf{r}) = -\nabla\phi_E(\mathbf{r}) = -\frac{\mu(\mathbf{r})}{e}\mathbf{g}(\mathbf{r})$$

when the boundary conditions are symmetric about the magnetic equator. ϕ_E is the electrostatic potential, $\mathbf{g}$ is the gravitational acceleration, and $\mu(\mathbf{r})$ is defined by

$$\mu(\mathbf{r}) = (\Sigma_j Z_j m_j n_j/kT_j)/(\Sigma_j Z_j^2 n_j/kT_j). \tag{A1}$$

The summations in formula (A1) are to be taken over all kinds of particles with mass m_j, density n_j, charge $Z_j e$ and temperature T_j; k is the Boltzmann constant. This

electric field assures the quasi-neutrality in the exospheric plasma. The zero-current condition is automatically satisfied as a consequence of the same boundary conditions at both intersection points of the magnetic field line with the baropause.

For a two constituent ion-exosphere in which the electrons and ions have the same temperature ($T_e = T_i$), the electrostatic potential is also given by the Pannekoek-Rosseland formula

$$\phi_E(\mathbf{r}) = -\frac{m_i - m_e}{2e}\,\phi_g(\mathbf{r}),$$

where ϕ_g denotes the gravitational potential.

Under the assumption that the guiding center approximation is valid in the exosphere, the motion of a charged particle with mass m and velocity v can be determined by (i) the law of conservation of energy

$$mv^2(\mathbf{r}) + (m_i + m_e)\,\phi_g(\mathbf{r}) = \text{const} \tag{A2}$$

and (ii) the first adiabatic invariant.

$$v^2(\mathbf{r})\sin^2\theta(\mathbf{r})/B(\mathbf{r}) = \text{const}, \tag{A3}$$

where θ is the pitch angle of the particle; i.e., the angle between the magnetic field **B** and the velocity vector of the particle.

The particles, moving along a magnetic field line can be arranged in four classes. The different regions in phase space, corresponding to each of these classes can be

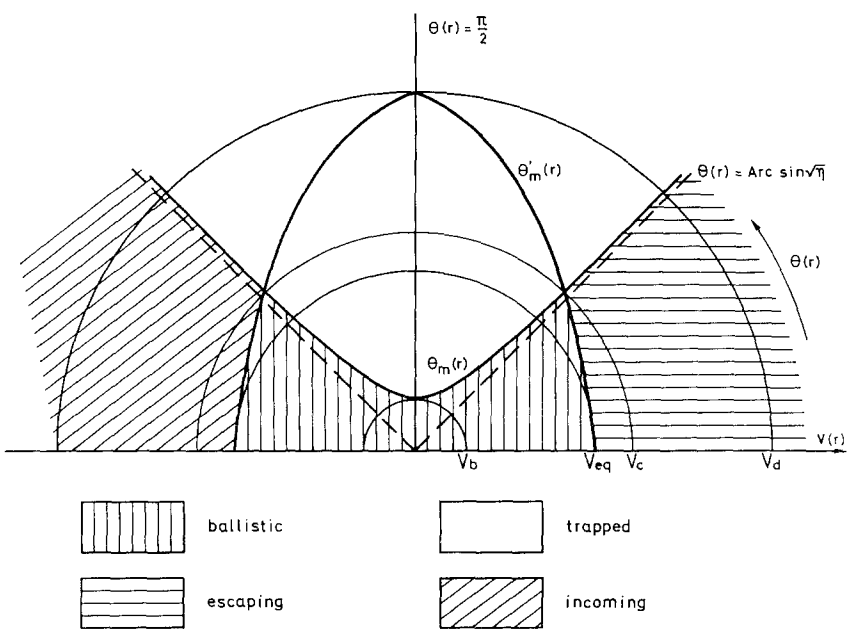

Fig. 19. Classes of particles in the velocity plane.

determined by means of the basic relations (A2) and (A3), and are illustrated in Figure 19 where the following notations are used

$$v_b^2(\mathbf{r}) = \varkappa\eta(1-y)/(1-\eta);$$
$$v_{eq}^2(\mathbf{r}) = \varkappa(y-y_{eq});$$
$$v_c^2(\mathbf{r}) = \varkappa[y-y_{eq}+a(1-y)]/(1-a);$$
$$v_d^2(\mathbf{r}) = \mu\varkappa(y-y_{eq})/(\mu-1);$$
$$\theta_m(\mathbf{r}) = \arcsin[\eta[1+\varkappa(1-y)/v^2(\mathbf{r})]]^{1/2};$$
$$\theta'_m(\mathbf{r}) = \arcsin[\mu[1-\varkappa(y-y_{eq})/v^2(\mathbf{r})]]^{1/2};$$

with

$$\varkappa = -\frac{m_i+m_e}{m}\phi_g(\mathbf{r}_0) > 0;$$
$$y = r_0/r; \qquad y_{eq} = r_0/r_{eq}$$
$$\eta = B(\mathbf{r})/B(\mathbf{r}_0) < 1; \qquad \mu = B(\mathbf{r})/B(\mathbf{r}_{eq}) > 1; \qquad a = B(\mathbf{r}_{eq})/B(\mathbf{r}_0) < 1$$

and where $\mathbf{r}_0$ and $\mathbf{r}_{eq}$ determine the intersection point of the magnetic field line through $\mathbf{r}$, with the baropause and the magnetic equator, respectively; $\mathbf{r}_0$ and $\mathbf{r}$ lie in the same hemisphere.

First of all there are the so-called *ballistic particles* which emerge from the barosphere and which do not have enough kinetic energy to reach the equator or which are reflected magnetically before reaching the equator. These particles will spiral up in the exosphere and fall back in the same hemisphere. For a Maxwellian velocity distribution at the exobase their number density is given by

$$n_B(\mathbf{r}) = 2n_0 e^{-q}\{K_2(V_{eq}) - AK_2(Xp^{-1/2}) + B[W_2(V_{eq}\sigma^{-1/2}) - W_2(X\sigma^{-1/2})]\} \qquad \text{(A4)}$$

with

$$q = \Lambda(1-y), \qquad \Lambda = \frac{m}{2kT_0}\varkappa = -\frac{m_i+m_e}{2kT_0}\phi_g(\mathbf{r}_0) > 0$$
$$V_{eq} = (m/2kT_0)^{1/2} v_{eq}(\mathbf{r}) = \Lambda(y-y_{eq})$$
$$X^2 = \Lambda\left[(y-y_{eq}) - \frac{a\sigma}{1-a}(1-y)\right]; \qquad \sigma = \mu - 1$$
$$A = p^{1/2}\exp(-\eta q/p); \qquad p = 1-\eta$$
$$B = \sigma^{1/2}\exp(-\mu V_{eq}^2/\sigma).$$

The functions $K_2(z)$ and $W_2(z)$ are defined by

$$K_2(z) = \frac{2}{\pi^{1/2}}\int_0^z \exp(-t^2)\,t^2\,dt = \tfrac{1}{2}\mathrm{erf}(z) - \frac{z}{\pi^{1/2}}\exp(-z^2)$$

$$W_2(z) = \frac{2}{\pi^{1/2}}\int_0^z \exp(t^2)\,t^2\,dt - \frac{1}{\pi^{1/2}}[z - D(z)]\exp(z^2),$$

where erf (z) and $D(z)$ are, respectively the error-function and Dawson's integral (Abramowitz and Stegun, 1964). Note that the number density is sometimes (Chamberlain, 1963) expressed by means of the incomplete gamma function $\gamma(\frac{3}{2}, x) = \sqrt{\pi} K_2(\sqrt{x})$.

The other group of particles emerging from the barosphere have sufficient kinetic energy and a proper pitch angle to reach the magnetic equator. Although these particles are still bounded to the Earth we will call them '*escaping*' *particles* since they leave one hemisphere and re-enter into the barosphere at the other hemisphere where they will be called '*incoming*' *particles*. Their density and flux are given, respectively, by

$$n_E(r) = n_I(r) = \tfrac{1}{2} n_0 e^{-q} [1 - A] - \tfrac{1}{2} n_B(r), \tag{A5}$$

where $n_B(r)$ is defined by (A4)
and

$$F_E(r) = -F_I(r) = n_0 (kT_0/2\pi m)^{1/2} \eta a^{-1} \{\exp[-A(1 - y_{eq})] + - (1 - a) \exp[-A(1 - y_{eq})/(1 - a)]\}. \tag{A6}$$

Finally there can exist *trapped particles* which bounce up and down between two mirror points in the ion-exosphere. Under the assumption of statistical equilibrium their density can be calculated by

$$n_T(r) = n_0 A e^{-q}. \tag{A7}$$

When all classes of particles are completely filled the total density is given by the barometric law

$$n(r) = n_B(r) + n_E(r) + n_I(r) + n_T(r) = n_0 e^{-q} \tag{A8}$$

applicable to the case of diffusive equilibrium.

Acknowledgements

The authors are very grateful to Prof. M. Nicolet for the interest he has taken in this work and for the support and encouragement he has given us.

References

Aamodt, R. E. and Case, K. M.: 1962, *Phys. Fluids* **5**, 1019–1021.

Abramowitz, M. and Stegun, I. A. (eds.): 1970, *Handbook of Mathematical Functions*, National Bureau of Standards, Applied Mathematics Series, No. 55 (U.S. Government Printing Office), Chap. 7, p. 295.

Angerami, J. J. and Thomas, J. O.: 1964, *J. Geophys. Res.* **69**, 4537–4560.

Aubry, M. P., Kivelson, M. G., McPherron, R. L., Russel, C. T., and Colburn, D. S.: 1972, *J. Geophys. Res.* **77**, 5487–5502.

Axford, W. I.: 1968, *J. Geophys. Res.* **73**, 6855–6859.

Axford, W. I. and Hines, C. O.: 1961, *Can. J. Phys.* **39**, 1433–1464.

Bame, S. J.: 1968, in B. M. McCormac (ed.), *Earth's Particles and Fields*, Reinhold, New York, pp. 373–383.

Bame, S. J., Asbridge, J. R., Felthauser, H. E., Hones, E. W., and Strong, I. B.: 1967, *J. Geophys. Res.* **72**, 113–129.

Banks, P. M.: 1971, *NATO Advanced Study Institute on Magnetosphere-Ionosphere Interactions*, Espedalen, Norway.
Banks, P. M. and Holzer, T. E.: 1968, *J. Geophys. Res.* **73**, 6846–6854.
Banks, P. M. and Holzer, T. E.: 1969a, *J. Geophys. Res.* **74**, 3734–3739.
Banks, P. M. and Holzer, T. E.: 1969b, *J. Geophys. Res.* **74**, 6304–6316.
Banks, P. M. and Holzer, T. E.: 1969c, *J. Geophys. Res.* **74**, 6317–6332.
Bates, D. R. and Patterson, T. N. L.: 1961, *Planetary Space Sci.* **5**, 257–273.
Bauer, S. J.: 1966, in J. Frihagen (ed.), *Electron Density Profiles in Ionosphere and Exosphere*, North-Holland Publishing Company, Amsterdam, pp. 270–280.
Bauer, S. J.: 1969, *Proc. Inst. Elec. Electron. Engrs.* **57**, 1114–1118.
Bertaux, J. L. and Blamont, J. E.: 1973, *J. Geophys. Res.* **78**, 80–91.
Biutner, E. K.: 1958, *Soviet Astronomy* **2**, 528–537.
Biutner, E. K.: 1959, *Soviet Astronomy* **3**, 92–102.
Block, L. P.: 1972, *Cosmic Electrodyn.* **3**, 349–376.
Brace, L. H., Reddy, B. M., and Mayr, H. G.: 1967, *J. Geophys. Res.* **72**, 265–283.
Brace, L. H., Mayr, H. G., and Mahajan, K. K.: 1970, *J. Atmospheric Terrest. Phys.* **32**, 1945–1957.
Brandt, J. C. and Chamberlain, J. W.: 1960, *Phys. Fluids* **3**, 485–486.
Brinkmann, R. T.: 1970, *Planetary Space Sci.* **18**, 449–478.
Brinkmann, R. T.: 1971, *Planetary Space Sci.* **19**, 791–794. 1971.
Brinton, H. C., Grebowsky, J. M., and Mayr, H. G.: 1971, *J. Geophys. Res.* **76**, 3738–3745.
Bryan, G. H.: 1900, *Proc. Roy. Soc. London* **66**, 335–336; 1900, *Nature* **62**, 189.
Bryan, G. H.: 1901, *Phil. Trans.* **A274**, 1–24.
Burch, J. L.: 1968, *J. Geophys. Res.* **73**, 3585–3591.
Burke, J. A.: 1969, *Monthly Notices Roy. Astron. Soc.* **145**, 487–492.
Carpenter, D. L.: 1966, *J. Geophys. Res.* **71**, 693–709.
Carpenter, D. L.: 1970, *J. Geophys. Res.* **75**, 3837–3847.
Carpenter, D. L. and Park, C. G.: 1973, *Rev. Geophys. Space Phys.* **11**, 133–154.
Chamberlain, J. W.: 1961, *Physics of the Aurora and Airglow*, Academic Press, New York, p. 704.
Chamberlain, J. W.: 1963, *Planetary Space Sci.* **11**, 901–960.
Chamberlain, J. W.: 1969, *Astrophys. J.* **155**, 711–714.
Chamberlain, J. W. and Campbell, F. J.: 1967, *Astrophys. J.* **149**, 687–705.
Chamberlain, J. W. and Smith, G. R.: 1971, *Planetary Space Sci.* **19**, 675–684.
Chappell, C. R.: 1972, *Rev. Geophys. Space Phys.* **10**, 951–979.
Chappell, C. R., Harris, K. K., and Sharp, G. W.: 1970a, *J. Geophys. Res.* **75**, 50–56.
Chappell, C. R., Harris, K. K., and Sharp, G. W.: 1970b, *J. Geophys. Res.* **75**, 3848–3861.
Chappell, C. R., Harris, K. K., and Sharp, G. W.: 1971, *J. Geophys. Res.* **76**, 7632–7647.
Chase, L. M.: 1970, *J. Geophys. Res.* **75**, 7128–7139.
Chew, G. F., Goldberger, M. L., and Low, F. E.: 1956, *Proc. Roy. Soc. London* **A236**, 112–118.
Choy, L. W., Arnoldy, R. L., Potter, W., Kintner, P., and Cahill, J. L., Jr.: 1971, *J. Geophys. Res.* **76**, 8279–8298.
Colin, L. and Dufour, S. W.: 1968, *J. Geophys. Res.* **73**, 2967–2984.
Cook, S. R.: 1900, *Astrophys. J.* **11**, 36–43.
DeForest, S. E. and McIlwain, C. E.: 1971, *J. Geophys. Res.* **76**, 3587–3611.
Dessler, A. J. and Cloutier, P. A.: 1969, *J. Geophys. Res.* **74**, 3730–3733.
Dessler, A. J. and Michel, F. C.: 1966, *J. Geophys. Res.* **71**, 1421–1426.
Donahue, T. M.: 1971, *Rev. Geophys. Space Phys.* **9**, 1–9.
Donahue, T. M. and McAfee, J. R.: 1964, *Planetary Space Sci.* **12**, 1045–1054.
Dungey, J. W.: 1961, *Phys. Rev. Letters* **6**, 47–48.
Dungey, J. W.: 1967, in J. W. King and W. S. Newman (eds.), *Solar-Terrestrial Physics*, Academic Press, London, pp. 91–106.
Eviatar, A., Lenchek, A. M., and Singer, S. F.: 1964, *Phys. Fluids* **7**, 1775–1779.
Fahr, H. J.: 1970, *Planetary Space Sci.* **18**, 823–834.
Fahr, H. J.: 1971, in J. Verniani (ed.), *Physics of the Upper Atmosphere*, Editrice Compositori, Bologna, pp. 348–366.
Feldstein, Y. I. and Starkov, G. V.: 1970, *Planetary Space Sci.* **18**, 501–508.
Frank, L. A. and Ackerson, K. L.: 1971, *J. Geophys. Res.* **76**, 3612–3643.
Gliddon, J. E. C.: 1963, *J. Atmospheric Terrest. Phys.* **25**, 175–177.

Godart, M.: 1962, *Aeronomica Acta* **A16**.
Gringauz, K. I., Bezrukikh, V. V., Ozerov, V. D., and Rybchinskii, R. E.: 1960a, *Soviet Phys. Doklady* **5**, 361–364.
Gringauz, K. I., Kurt, V. G., Moroz, V. I., and Shklovskii, I. S.,: 1960b, *Soviet Astron. AJ.* **4**, 680–695.
Hagenbuch, K. M. and Hartle, R. E.: 1969, *Phys. Fluids* **12**, 1551–1559.
Hanson, W. B. and Patterson, T. N. L.: 1963, *Planetary Space Sci.* **11**, 1035–1052.
Hartle, R. E.: 1969, *Phys. Fluids* **12**, 455–462.
Hartle, R. E.: 1971, *Phys. Fluids* **14**, 2592–2598.
Hays, P. B. and Liu, V. C.: 1965, *Planetary Space Sci.* **13**, 1185–1212.
Heikkila, W. J.: 1972, *Space Research XII* **2**, 1343–1355.
Herring, J. and Kyle, L.: 1961, *J. Geophys. Res.* **66**, 1980–1982.
Hodges, R. R., Jr. and Johnson, F. S.: 1968, *J. Geophys. Res.* **73**, 7307–7317.
Hoffman, J. H.: 1968, *Trans. Am. Geophys. Union* **49**, 253.
Hoffman, J. H.: 1970, *Int. J. Mass. Spectrom. Ion Phys.* **4**, 315–322.
Hoffman, J. H.: 1971, *Trans. Am. Geophys. Union* **52**, 301.
Holzer, T. E., Fedder, J. A., and Banks, P. M.: 1971, *J. Geophys. Res.* **76**, 2453–2468.
Hones, E. W., Jr.: 1968, in R. L. Carovillano, J. F. McClay, and H. R. Radoski (eds.), *Physics of the Magnetosphere*, D. Reidel Publ. Co., Dordrecht, Holland, pp. 392–408.
Hones, E. W. and Bergeson, J. E.: 1965, *J. Geophys. Res.* **70**, 4951–4958.
Hones, E. W., Jr., Asbridge, J. R., Bame, S. J., and Singer, S.: 1971, *J. Geophys. Res.* **76**, 63–87.
Hultqvist, B.: 1971, *Planetary Space Sci.* **19**, 749–759.
Hultqvist, B.: 1972, in E. R. Dyer (ed.), *Solar-Terrestrial Physics/1970*, Part IV, Reidel Publ. Co., Dordrecht, Holland, pp. 176–198.
Jeans, J. H.: 1925, *The Dynamical Theory of Gases* (4th ed.), Cambridge University Press, Cambridge, p. 444.
Johnson, F. S.: 1960a, *J. Geophys. Res.* **65**, 577–584.
Johnson, F. S.: 1960b, *J. Geophys. Res.* **65**, 2571–2575.
Johnson, F. S.: 1961, *Astrophys. J.* **133**, 701–705.
Johnson, F. S. and Fish, R. A.: 1960, *Astrophys. J.* **131**, 502–515.
Jones, J. E.: 1923, *Trans. Cambridge Phil. Soc.* **22**, 535–556.
Kamiyama, H.: 1968, *Rept. Ionosph. Space Res. Japan* **22**, 249–256.
Kamiyama, H. and Takaki, H.: 1966, *J. Geomag. Geoelec.* **18**, 1–11.
Kindel, J. M. and Kennel, C. F.: 1971, *J. Geophys. Res.* **76**, 3055–3078.
Knight, S.: 1973, *Planetary Space Sci.* **21**, 741–750.
Lemaire, J.: 1972a, *J. Atmospheric Terrest. Phys.* **34**, 1647–1658.
Lemaire, J.: 1972b, *Space Research XII*, 1414–1416.
Lemaire, J.: 1974, 'Rotating Ion-Exospheres', submitted to *Planetary Space Sci.*
Lemaire, J. and Scherer, M.: 1969, *Compt. Rend. Acad. Sci. Paris* **269**, 666–669.
Lemaire, J. and Scherer, M.: 1970, *Planetary Space Sci.* **18**, 103–120.
Lemaire, J. and Scherer, M.: 1971, *Phys. Fluids* **14**, 1683–1694.
Lemaire, J. and Scherer, M.: 1972a, *Phys. Fluids* **15**, 760–766.
Lemaire, J. and Scherer, M.: 1972b, *Bull. Acad. Sci. Belg.* **58**, 502–512.
Lemaire, J. and Scherer, M.: 1973a, *Rev. Geophys. Space Phys.* **11**, 427–468.
Lemaire, J. and Scherer, M.: 1973b, *Planetary Space Sci.* **21**, 281–289.
Lew, S. K.: 1967, Ph.D. Thesis, University of California, Los Angeles.
Lew, S. K. and Venkateswaran, S. V.: 1965, *J. Atmospheric Sci.* **22**, 623–635.
Lew, S. K. and Ventkateswaran, S. V.: 1966, *J. Atmospheric Sci.* **23**, 817–819.
Liwshitz, M.: 1966, *J. Atmospheric Sci.* **23**, 816–817.
Liwshitz, M.: 1967, *J. Geophys. Res.* **72**, 285–293.
Liwshitz, M. and Singer, S. F.: 1966, *Planetary Space Sci.* **14**, 541–561.
MacMahon, A.: 1965, *Phys. Fluids* **8**, 1840–1845.
Mange, P.: 1960, *J. Geophys. Res.* **65**, 3833–3834.
Mange, P.: 1972, in E. R. Dyer (ed.), *Solar and Terrestrial Physics/1970*, Part IV, D. Reidel Publ. Co., Dordrecht, Holland, pp. 68–86.
Marubashi, K.: 1970a, *Rept. Ionospheric Space Res. Japan* **24**, 322–346.
Marubashi, K.: 1970b, *J. Rad. Res. Lab.* **17**, 335–416.

Mayr, H. G., Fontheim, E. G., Brace, L. H., Brinton, H. C., and Taylor, H. A., Jr.: 1972, *J. Atmospheric Terrest. Phys.* **34**, 1659–1680.
McAfee, J. R.: 1965, Ph.D. Thesis, University of Pittsburgh.
McAfee, J. R.: 1967, *Planetary Space Sci.* **15**, 599–609.
McIlwain, C. E.: 1972, in B. M. McCormac (ed.), *Earth's Magnetospheric Processes*, Reidel Publ. Co., Dordrecht, Holland, pp. 268–279.
Meier, R. R. and Mange, P.: 1970, *Planetary Space Sci.* **18**, 803–821.
Melrose, D. B.: 1967, *Planetary Space Sci.* **15**, 381–393.
Milne, E. A.: 1923, *Trans. Cambridge Phil. Soc.* **22**, 483–517.
Mitra, S. K. and Banerjee, A. K.: 1939, *Indian J. Phys.* **13**, 107–144.
Moffett, R. J. and Hanson, W. B.: 1973, *J. Atmospheric Terrest. Phys.* **35**, 207–222.
Ness, N. F.: 1965, *J. Geophys. Res.* **70**, 2989–3005.
Nicolet, M.: 1961, *J. Geophys. Res.* **66**, 2263–3364.
Nicolet, M.: 1964, in H. Odishaw (ed.), *Research in Geophysics*, Vol. I, MIT Press, Cambridge, Mass., pp. 243–275.
Nishida, A.: 1966, *J. Geophys. Res.* **71**, 5669–5679.
Öpik, E. J.: 1963, *Geophys. J.* **7**, 490–509.
Öpik, E. J. and Singer, S. F.: 1959, *Phys. Fluids* **2**, 653–655.
Öpik, E. J. and Singer, S. F.: 1960, *Phys. Fluids* **3**, 486–488.
Öpik, E. J. and Singer, S. F.: 1961, *Phys. Fluids* **4**, 221–233.
Pannekoek, A.: 1922, *Bull. Astron. Inst. Neth.* **1**, 107–118.
Patterson, T. N. L.: 1966, *Planetary Space Sci.* **14**, 425–431.
Pickel'ner, S. B.: 1950, *Doklady Akad. Nauk SSSR* **72**, 255–258.
Quessette, J. A.: 1972, *J. Geophys. Res.* **77**, 2997–3000.
Roederer, J. G.: 1969, *Rev. Geophys.* **7**, 77–96.
Rosseland, S.: 1924, *Monthly Notices Roy. Astron. Soc.* **84**, 720–728.
Rycroft, M. J. and Burnell, S. J.: 1970, *J. Geophys. Res.* **75**, 5600–5604.
Rycroft, M. J. and Thomas, J. O.: 1970, *Planetary Space Sci.* **18**, 65–80.
Schield, M. A. and Frank, L. A.: 1970, *J. Geophys. Res.* **75**, 5401–5414.
Serbu, G. P. and Maier, E. J. R.: 1966, *J. Geophys. Res.* **71**, 3755–3766.
Serbu, G. P. and Maier, E. J. R.: 1970, *J. Geophys. Res.* **75**, 6102–6113.
Shen, C. S.: 1963, *J. Atmospheric Sci.* **20**, 69–72.
Singer, S. F.: 1960a, *Planetary Space Sci.* **2**, 165–173.
Singer, S. F.: 1960b, *J. Geophys. Res.* **65**, 2577–2580.
Spitzer, L., Jr.: 1949, in G. P. Kuiper (ed.), *The Atmospheres of the Earth and Planets*, Univ. Chicago Press, Ill., pp. 213–249.
Spitzer, L., Jr.: 1956, *Physics of Fully Ionized Gases*, Interscience Publish. Co., New York, p. 105.
Stoney, G. J.: 1868, *Proc. Roy. Soc. London* **17**, 1–57.
Stoney, G. J.: 1898, *Astrophys. J.* **7**, 25–55.
Stoney, G. J.: 1900a, *Astrophys. J.* **11**, 251–258.
Stoney, G. J.: 1900b, *Astrophys. J.* **11**, 357–372.
Stoney, G. J.: 1900c, *Astrophys. J.* **12**, 201–207; 1900c, *Proc. Roy. Soc. London* **67**, 286–291.
Stoney, G. J.: 1904, *Astrophys. J.* **20**, 69–78.
Strobel, D. F. and Weber, E. J.: 1972, *J. Geophys. Res.* **77**, 6864–6869.
Taylor, H. A., Jr.: 1971a, 'Observed Solar Geomagnetic Control of the Ionosphere: Implications for the Reference Ionospheres', GSFC X-621-71-232.
Taylor, H. A., Jr.: 1971b, *Planetary Space Sci.* **19**, 77–93.
Taylor, H. A., Jr.: 1972, *Planetary Space Sci.* **20**, 1593–1605.
Taylor, H. A., Jr. and Walsh, W. J.: 1972, *J. Geophys. Res.* **77**, 6716–6723.
Taylor, H. A., Jr., Brinton, H. C., and Smith, C. R.: 1965, *J. Geophys. Res.* **70**, 5769–5781.
Taylor, H. A., Jr., Brinton, H. C., Pharo, M. W., III, and Rahman, N. K.: 1968, *J. Geophys. Res.* **73**, 5521–5533.
Taylor, H. A., Jr., Brinton, H. C., Carpenter, D. L., Bonner, F. M., and Heyborne, R. L.: 1969, *J. Geophys. Res.* **74**, 3517–3528.
Thomas, J. O., Rycroft, M. J., Colin, L., and Chan, K. L.: 1966, in J. Frihagen (ed.), *Electron Density Profiles in the Ionosphere and Exosphere*, North-Holland, Amsterdam, pp. 322–257.
Tulunay, Y. K.: 1972, *Planetary Space Sci.* **20**, 1299–1307.

Tulunay, Y. K.: 1973, *J. Atmospheric Terrest. Phys.* **35**, 233–254.
Tulunay, Y. K. and Hughes, A. R. W.: 1973, *J. Atmospheric Terrest. Phys.* **35**, 153–163.
Tulunay, Y. K. and Sayers, J.: 1971, *J. Atmospheric Terrest. Phys.* **33**, 1737–1761.
Vasyliunas, V. M.: 1970, in G. Sklovi (ed.), *The Polar Ionosphere and Magnetospheric Processes*, Gordon and Breach, New York, pp. 25–47.
Venkateswaran, S. V.: 1971, *Planetary Space Sci.* **19**, 275.
Vidal-Madjar, A. and Bertaux, J. L.: 1972, *Planetary Space Sci.* **20**, 1147–1162.
Vondrack, R. R., Anderson, H. R., and Spiger, R. J.: 1971, *J. Geophys. Res.* **76**, 7701–7713.
Waterston, J. J.: 1846, *Proc. Roy. Soc. London* **5**, 604.
Waterston, J. J.: 1892, *Phil. Trans. Roy. Soc. London* **A183**, 1–80.
Zmuda, A. J., Armstrong, J. C., and Heuring, F. T.: 1970, *J. Geophys. Res.* **75**, 4757–4762.